Molecular Characterization of Vegetative Incompatibility Genes That Restrict Hypovirus Transmission in the Chestnut Blight Fungus *Cryphonectria parasitica*

Gil H. Choi,* Angus L. Dawe,†,‡ Alexander Churbanov,† Myron L. Smith,§ Michael G. Milgroom, and Donald L. Nuss*,[1]**

*Institute for Bioscience and Biotechnology Research, University of Maryland, Rockville, Maryland 20850, †Department of Biology and ‡Molecular Biology Program, New Mexico State University, Las Cruces, New Mexico 88003, §Department of Biology, Carleton University, Ottawa, Ontario K1S 5B6, Canada, and **Department of Plant Pathology and Plant-Microbe Biology, Cornell University, Ithaca, New York 14853

ABSTRACT Genetic nonself recognition systems such as vegetative incompatibility operate in many filamentous fungi to regulate hyphal fusion between genetically dissimilar individuals and to restrict the spread of virulence-attenuating mycoviruses that have potential for biological control of pathogenic fungi. We report here the use of a comparative genomics approach to identify seven candidate polymorphic genes associated with four vegetative incompatibility (*vic)* loci of the chestnut blight fungus *Cryphonectria parasitica*. Disruption of candidate alleles in one of two strains that were heteroallelic at *vic2*, *vic6*, or *vic7* resulted in enhanced virus transmission, but did not prevent barrage formation associated with mycelial incompatibility. Detailed characterization of the *vic6* locus revealed the involvement of nonallelic interactions between two tightly linked genes in barrage formation, heterokaryon formation, and asymmetric, gene-specific influences on virus transmission. The combined results establish molecular identities of genes associated with four *C. parasitica vic* loci and provide insights into how these recognition factors interact to trigger incompatibility and restrict virus transmission.

ENDOGENOUS mycoviruses have been reported to alter the ability of plant pathogenic fungi to cause disease (reviews by Nuss 2005, 2010; Ghabrial and Suzuki 2009; Pearson *et al.* 2009). These mycovirus infections generally result in reduced virulence, termed hypovirulence, and offer the potential for development of biological control strategies for a range of pathogenic fungi. Unlike viruses of plants and animals, viruses of fungi uniformly lack an extracellular phase in their replication cycle (Wickner 2001). Transmission is limited to intracellular mechanisms such as cytoplasmic exchange during hyphal anastomosis (fusion of hyphae) or transmission through asexual spores. While mycoviruses are able to move freely through the hyphal network that comprises a fungal colony, transmission between different strains of the same fungal species is often regulated by a genetic nonself recognition system governed by vegetative incompatibility (Glass and Kuldau 1992; Leslie 1993; Glass *et al.* 2000; Saupe 2000). Vegetative incompatibility may be evident when mycelia of genetically distinct conspecific strains grow together and form a barrage, or demarcation line, along the zone of contact. It can also be assayed by allowing conspecific strains to fuse to form a heterokaryon (cells having more than one nuclear type); incompatible heterokaryons grow slowly and with an abnormal morphology or exhibit no growth. While often used interchangeably, barrage formation and heterokaryon incompatibility are not

doi: 10.1534/genetics.111.133983
Manuscript received August 31, 2011; accepted for publication October 15, 2011
Available freely online through the author-supported open access option.
Supporting information is available online at http://www.genetics.org/content/suppl/2011/10/20/genetics.111.133983.DC1.
Sequence data from this article for the candidate *vic* genes have been deposited with the EMBL/GenBank Data Libraries under the following accession nos.: *vic6-1*, JN367268; *vic6-2*, JN256666; *pix6-1*, JN367270; *pix6-2*, JN367269; *vic2-1*, JN367272; *vic2-2*, JN367271; *vic2a-1*, JN367274; *vic2a-2*, JN367273; *vic4-1*, JN367275; and *vic4-2*, JN367276.
[1]Corresponding author: Institute for Bioscience and Biotechnology Research, University of Maryland, 9600 Gudelsky Dr., Rockville, MD 20850. E-mail: dnuss@umd.edu

necessarily concordant, but both represent manifestations of vegetative incompatibility (review in Smith *et al.* 2006) wherein incompatible interactions result in localized programmed cell death (PCD) (Jacobson *et al.* 1998; Biella *et al.* 2002) that restricts exchange of cellular contents (Leslie and Zeller 1996) and transmission of viruses, transposable elements, and senescence plasmids (Caten 1972; Hartl *et al.* 1975).

The influence of fungal vegetative incompatibility on the transmission and efficacy of virulence-attenuating mycoviruses for biological control has been studied most extensively for hypoviruses responsible for hypovirulence of the chestnut blight fungus *Cryphonectria parasitica*. Results of field studies conducted in both Europe and North America generally indicate that hypovirus transmission and biological control are more effective in *C. parasitica* populations that exhibit lower vegetative incompatibility diversity (Anagnostakis *et al.* 1986; Heiniger and Rigling 1994; Robin *et al.* 2000, 2009; Milgroom and Cortesi 2004). The vegetative incompatibility system in *C. parasitica* is controlled by at least six genetic vegetative incompatibility (*vic*) loci with only two alleles known at each locus (Anagnostakis 1982b; Huber 1996; Cortesi and Milgroom 1998). Hyphae of *C. parasitica* strains that contain the same alleles at all *vic* loci freely fuse and support virus transmission. Hyphae of strains that contain different alleles at one or more *vic* loci undergo incompatible reactions that result in cell death and restriction of virus transmission. Genotypes corresponding to all combinations of alleles at six *vic* loci have been identified and are represented by a collection of corresponding tester stains (Cortesi and Milgroom 1998). This has allowed analysis of the influence of differences at specific *vic* loci on virus transmission, leading to the confirmation of allele-specific influences on the frequency and symmetry of virus transmission (Huber and Fulbright 1994; Cortesi *et al.* 2001). These differences are correlated with allele-specific differences in the rate of PCD associated with incompatible interactions, in which delayed PCD allows greater virus transmission (Biella *et al.* 2002).

Although vegetative incompatibility is a common phenomenon in filamentous ascomycete fungi, only a limited number of genes controlling this process have been characterized at the molecular level in two species: *Neurospora crassa* and *Podospora anserina* (reviewed in Saupe *et al.* 2000; Glass and Dementhon 2006; Pinan-Lucarre *et al.* 2007; Paoletti and Saupe 2009). Heterokaryon incompatibility (*het*) genes in these two species are characterized by significant allelic polymorphism and generally encode proteins that contain a conserved HET domain (Pfam: PF06985). The variable protein domains determine specificity while the HET domain may transduce the recognition signal to activate PCD (Paoletti and Clavé 2007). The variable and HET domains can be incorporated into the same protein or reside on tightly linked gene products (Glass and Dementhon 2006; Kaneko *et al.* 2006; Micali and Smith 2006; Paoletti and Saupe 2009).

Five of the *C. parasitica vic* loci have been linked to molecular markers on a genetic linkage map (Kubisiak and Milgroom 2006). We hypothesized that, if the *C. parasitica vic* system resembles the nonself recognition systems that operate in *N. crassa* and *P. anserina*, then the *C. parasitica vic* loci should be identifiable as regions of hypervariability located near the linked markers. We confirmed this prediction by identifying seven candidate polymorphic genes associated with four *vic* loci through comparative analysis of the genome sequences of two *C. parasitica* strains, EP155 (reference genome sequence) and EP146, that were genetically determined to have allelic differences at *vic2*, *vic4*, *vic6*, and *vic7*. A role in restriction of virus transmission was demonstrated by disruption of the polymorphic candidate genes associated with the *vic* loci previously implicated by genetic analysis as restricting virus transmission, *vic2*, *vic6*, and *vic7* (Cortesi *et al.* 2001). Nonallelic interactions between two tightly linked genes at the *vic6* locus were shown to trigger incompatibility and influence the frequency and symmetry of virus transmission. RNA silencing was recently shown to serve as an effective antiviral defense mechanism in *C. parasitica* (Segers *et al.* 2007; Zhang *et al.* 2008; Sun *et al.* 2009b). The results of this study also strengthen an emerging view of the complementary nature of RNA silencing and the *vic* system in fungal antiviral defense at the cellular and population levels, respectively.

Materials and Methods

Fungal strains and growth conditions

The *C. parasitica* strains used in this study (Table 1) were maintained on potato dextrose agar (PDA; Difco, Detroit) at 22°–24° with a 12-h/12-h light/dark cycle and a light intensity of 1300–1600 lx. EP155 (ATCC 38755), used for generation of the reference *C. parasitica* genome sequence (http://genome.jgi-psf.org/Crypa2/Crypa2.home.html), is a virulent, hypovirus-free orange pigment-producing strain isolated by Sandra Anagnostakis (Connecticut Agricultural Experiment Station, New Haven, CT) in 1977 from a canker on *Castanea dentata* (Marshall) Borkh. in a field plot in Bethany, Connecticut. Strain EP146 (ATCC 64671) is a virulent, hypovirus-free, brown pigment-producing strain isolated in 1976 from the George Washington National Forest near Franklin, West Virginia by William MacDonald (West Virginia University, Morgantown, WV). This strain was chosen for resequencing because of mating type and pigmentation differences with the reference genome strain EP155 and previous use in laboratory and field studies. (Chen *et al.* 1993; Root *et al.* 2005).

Vegetative incompatibility genotyping

Vegetative incompatibility genotyping was performed by pairing the *C. parasitica* strain of interest with each of the 64 European (EU) tester strains described by Cortesi and Milgroom (1998) on agar medium amended with bromocresol green pH indicator dye as described (Cortesi and Milgroom 1998).

Table 1 *Cryphonectria parasitica* strains used in this study

Strain	Characteristic(s)	Source/reference
EP155	Mating type *MAT-2*; *vic* genotype *2211-22*	ATCC 38755
EP146	Mating type *MAT-1*; *vic* genotype *2112-11*	ATCC 64671
DK80	EP155 genetic background; Δ*cpku80*	Lan *et al.* (2008)
DK80hygR	DK80 with hygromycin resistance	This study
DK80neoR	DK80 with G418 resistance	This study
DK80 Δ*vic2-2*	DK80 background; *vic2-2*::hygR	This study
DK80 Δ*vic6-2*	DK80 background; *vic6-2*::hygR	This study
DK80 Δ*vic7-2*	DK80 background; *vic7-2*::hygR	This study
DK80 Δ*pix6-2*	DK80 background; *pix6-2*::hygR	This study
DK80 Δ*pix6-2* Δ*vic6-2*	DK80 background; *pix6-2*::neoR, *vic6-2*::hygR	This study
EU-5	Tester strain for *vc* type EU-5 (isolate P1-11), *vic* genotype *2211-22*	Cortesi and Milgroom (1998)
EU-6	Tester strain for *vc* type EU-6 (isolate P1-6), *vic* genotype *2111-22*	Cortesi and Milgroom (1998)
EU-18	Tester strain for *vc* type EU-18 (isolate P24-33), *vic* genotype *2211-21*	Cortesi and Milgroom (1998)
EU-21	Tester strain for *vc* type EU-21 (isolate P10-18), *vic* genotype *2211-12*	Cortesi and Milgroom (1998)
EU-21hygR	EU-21 with hygromycin resistance	This study
EU-21neoR	EU-21 with G418 resistance	This study
EU-21 Δ*vic6-1*	EU-21 background; *vic6-1*::neoR	This study
EU-21 Δ*pix6-1*	EU-21 background; *pix6-1*::neoR	This study

vic genotypes are abbreviated as the alleles at each of the six known *vic* loci, *e.g.*, *2211-22* is the abbreviation for genotype *vic1-2*, *vic2-2*, *vic3-1*, *vic4-1*, *vic6-2*, *vic7-2* (Cortesi and Milgroom 1998).

Virus transmission assay

Virus transmission was assayed by placing a donor strain infected with hypovirus CHV-1/EP713 and a virus-free recipient strain 1 cm apart on PDA and incubating them at 22°–24° for 7 days. Virus transmission to the recipient strain can be detected by phenotypic conversion of the expanding edge of the recipient strain colony following contact of the two strains (see Figure 1 of Cortesi *et al.* 2001). Hypovirus CHV-1/EP713 infection was established in the different donor strains tested in this study by transfection of fungal spheroplasts with hypovirus CHV-1/EP713 transcripts generated *in vitro* from a full-length viral cDNA clone using the protocol developed by Chen *et al.* (1994).

Heterokaryon incompatibility assay

Heterokaryon incompatibility assays were done as described by Smith *et al.* (2006) with slight modifications. Briefly, strains were paired by placing 1- to 2-mm^3 blocks of agar containing actively growing mycelium ~2 mm apart on a cellophane membrane overlaid on top of PDA. The plates were incubated at 30° for 24 hr or until the paired colony margins overlapped by ~1 mm at which time the membrane with the paired colonies was transferred to PDA+hyg+G418 [PDA, 30 μg/ml hygromycin B (Roche, Laval, QC, Canada), and 20 μg/ml G418 (an analog of neomycin: BioShop Canada, Burlington, ON, Canada)]. The double-selection plates were incubated an additional 3–4 days at 30° before observation for heterokaryotic outgrowths. Mycelium from the edge of outgrowths or from the zone of confluence of paired colonies was subsequently transferred to PDA+hyg+G418 for growth rate measurements.

Genome sequencing and analysis

Genome sequence data for strain EP155, including gene models and predicted protein functional information, were obtained from the Joint Genome Institute of the U.S. Department of Energy (http://genome.jgi.psf.org/Crypa2/Crypa2.download.ftp.html). Data for strain EP146 were generated in the New Mexico State University (NMSU) Genome Sequencing Laboratory according to the Roche 454 GS FLX Titanium protocols for library preparation, emulsion PCR reaction, and sequencing (Margulies *et al.* 2005). Subsequently, quality-screened reads were mapped against the EP155 genome with Roche gsMapper v.2.5p1 software. Combined gsMapper alignments and EP155 genome data were then used to create a web-based interface using the freely available Generic Genome Browser (GBrowse) from the Generic Model Organism Database (http://gmod.org). Homology searches using specific gene sequences were performed using BLAST (http://blast.ncbi.nlm.nih.gov/Blast.cgi). GenBank accession numbers for the candidate *vic* genes are as follows: *vic6-1*, JN367268; *vic6-2*, JN256666; *pix6-1*, JN367270; *pix6-2*, JN367269; *vic2-1*, JN367272; *vic2-2*, JN367271; *vic2a-1*, JN367274; *vic2a-2*, JN367273; *vic4-1*, JN367275; and *vic4-2*, JN367276.

Small-scale genomic DNA isolation and disruption of candidate vic genes

C. parasitica strains were cultured on cellophane-overlaid PDA plates until the colony size became ~1.5–2 cm in diameter. Mycelia were gently removed and transferred to 2-ml screw-capped Sarstedt tubes containing 0.5 g of 0.5-mm zirconium beads in 400 μl extraction buffer (40 mM Tris-HCl, pH 8.0, 100 mM NaCl, 10 mM EDTA, 0.5% SDS). The tubes were shaken for 30 sec at 5000 rpm in a Mini BeadBeater (Biospec Products, Bartlesville, OK), cooled in ice, and subjected to two additional rounds of shaking and cooling. The samples were extracted with phenol/chloroform/iso-amyl alcohol (25/24/1) and the aqueous phase was collected for ethanol precipitation. After centrifugation, pellets were

resuspended in 10–40 μl of water depending on the pellet size.

Disruption of the candidate *vic* genes was performed according to the PCR-based strategy (Kuwayama *et al.* 2002; Sun *et al.* 2009a) with modifications. Three PCR products, which included a selectable marker and two flanking target gene-specific sequences, were generated in the first round of PCR. A second round of PCR was performed (30 cycles consisting of denaturation at 98° for 5 sec, annealing at 64° for 20 sec, and extension at 72° for 1.5 min) to assemble the three fragments using Phusion High-Fidelity DNA polymerase (New England Biolabs, Ipswich, MA) and two end oligonucleotide primers corresponding to the flanking gene-specific sequences. Transformation was performed according to the method of Churchill *et al.* (1990), followed by selection of putative transformants in the presence of 40 μg/ml of hygromycin or 20 μg/ml of G418. Putative disruptants were placed under intense constant light condition (~4000 lx) to promote asexual sporulation (Hillman *et al.* 1990) followed by the selection of uninucleate single conidial isolates on antibiotic-containing PDA to eliminate heterokaryons. Disruption of the candidate *vic* genes was confirmed in single-spore transformants by PCR analyses.

Results

Genotyping EP146 vic genes

Cortesi and Milgroom (1998) established a collection of 64 European *C. parasitica* isolates or "tester strains" that represent all possible genotypes arising from the six genetically identified *vic* loci, each with two alleles. *C. parasitica* strain EP155 (see Table 1), the strain used to generate the reference genome sequence (http://genome.jgi-psf.org/Crypa2/Crypa2.home.html), was previously shown to be compatible with tester strain EU-5 and thus have the genotype *2211-22*, where each number refers to the allele present at the respective *vic* loci, *i.e.*, *vic1-2*, *vic2-2*, *vic3-1*, *vic4-1*, *vic6-2*, and *vic7-2* (Cortesi and Milgroom 1998). The *vic* genotype for resequenced *C. parasitica* strain EP146 was determined by pairing with each of the 64 tester strains. Compatibility was observed with tester strain EU-17 (Figure 1) that has the *vic* genotype *2112-11*. Thus, strain EP146 differs from the reference strain EP155 at four *vic* loci: *vic2*, *vic4*, *vic6*, and *vic7*.

Polymorphism-based identification of C. parasitica vic gene alleles

The EP146 genome was sequenced to ~11× coverage (486.6 Mbp) using Roche 454 high-throughput sequencing technology. Raw reads (average length of 384 bp) were individually mapped onto the scaffolds composing the *C. parasitica* strain EP155 reference genome sequence within a searchable genome browser.

Kubisiak and Milgroom (2006) reported the construction of a *C. parasitica* linkage map based on a cross between Japanese isolate JA17 and Italian isolate P17-8 and identified

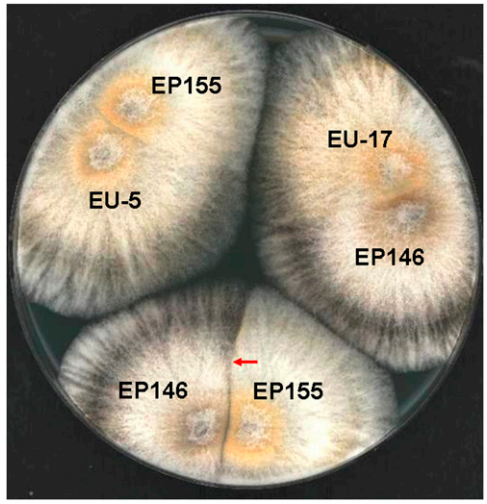

Figure 1 Vegetative incompatibility (*vic*) genotyping of *C. parasitica* strain EP146. Strains of *C. parasitica* that differ at one or more *vic* loci form barrage lines (a line of dead cells) when colonies of the two strains merge as observed for the pairing of strains EP155 and EP146 (barrage line indicated by red arrow at bottom of the culture plate). Cortesi and Milgroom (1998) established a collection of 64 *C. parasitica* tester strains that represent all possible genotypes arising from the six genetically determined *vic* loci. Strain EP155, the strain used for generation of the reference genome sequence (http://genome.jgi-psf.org/Crypa2/Crypa2.home.html), was previously reported (Cortesi and Milgroom 1998) to give a compatible reaction (fusion of hyphae with no barrage formation) with tester strain EU-5 (*vic* genotype *2211-22*) as shown at the left of the culture plate. Resequenced strain EP146 was found to be compatible with tester strain EU-17, as shown at the right side of the culture plate, and thus to have the *vic* genotype *2112-11*.

a number of markers linked to five of the known *vic* loci: *vic1*, *vic2*, *vic4*, *vic6*, and *vic7*. In this study, we updated the published linkage map by adding simple sequence repeat (SSR) markers mined from the EP155 reference genome sequence (Supporting Information, Table S1), using methods described in Kubisiak *et al.* (2007). We used the *vic*-linked markers generated in the JA17 × P17-8 mapping population as starting reference positions on the EP155 reference genome sequence assembly to screen for sequence polymorphisms with the 454-generated EP146 genome sequence that could correspond to candidate *vic* alleles.

vic2: Sequences corresponding to two markers in linkage group (LG)XIII shown previously to be closely linked to the *vic2* locus were identified on Scaffold 7 of the EP155 genome sequence assembly, version 2. The *vic2* locus was mapped 4.5 cM from marker C016_1800 on one side and 14.8 cM from SSR marker CpSI002 on the other side and found to cosegregate with marker P12_0475 (Figure 2A). Only one region of significant sequence polymorphism was identified between the CpSI002 and C016_1800 linkage markers on Scaffold 7. This consisted of a 10-kbp region that extended from position 1,661,000 to 1,671,000 and contained the *vic2* cosegregating marker P12_0475 at position 1,662,737. This 10-kbp polymorphic region contained two open reading frames (ORFs), one encoding a member of the patatin-like

phospholipase family [Pfam 01734 (Andrews *et al.* 1988)] and the other a protein related to a fungal plasma membrane SNARE Sec9 protein (reviewed in Hong 2005; Jahn and Scheller 2006) (Figure 2B). Remarkably, a comparison of the predicted amino acid sequences for these ORFs from strains EP155 and EP146 revealed that both were highly polymorphic [39% and 58% identity, respectively (Figure S1 and Figure S2)]. In contrast, the 2.7-kbp sequence separating the two ORFs showed only a moderate level of single-nucleotide polymorphisms and contained a 444-codon ORF encoding a helicase-like protein that was 99% identical in EP155 and EP146; high levels of sequence similarity were also found for proteins flanking this region. The patatin-like and sec9-like genes in strain EP155 were designated *vic2-2* and *vic2a-2*, respectively, while these genes in strain EP146 were designated candidate *vic* alleles *vic2-1* and *vic2a-1*, respectively.

vic4: The *vic4* locus was mapped between EP155 genome-specific SSR linkage markers CPG3 and CpSI116 on LGI that corresponded to positions 1,897,839 and 345,343, respectively, on Scaffold 4 (Figure S3), ~42.4 cM from the latter. Using the same strategy as described for the *vic2* locus, we identified a polymorphic region extending from position 1,075,432 to 1,077,374 that narrowly defined a single annotated ORF of 359 aa that contained a protein kinase c-like domain in the EP155 sequence (Figure 3). Interestingly, this sequence was replaced in the corresponding EP146 sequence contig by a larger ORF of 1628 aa that contained the classic NACHT-NTPase and WD repeat domains characteristic of a number of fungal heterokaryon incompatibility genes (Figure 4) (reviewed in Chevanne *et al.* 2010). The idiomorphic genes encoding the ORF with the protein kinase c-like domain in strain EP155 and the corresponding NACHT-NTPase/WD repeat-encoding gene in strain EP146 were designated candidate *vic* genes *vic4-1* and *vic4-2*, respectively.

vic6: The *vic6* locus was mapped by Kubisiak and Milgroom (2006) to reside 13.8 cM and 15.2 cM from linkage group XIV SSR linkage markers CpSI135 and CpSI136, respectively, which were located at positions 5,015,225 and 5,033,338, respectively, on Scaffold 3 (Figure S4). A 3710-bp region of sequence polymorphism was identified (Figure 5), extending from position 4,887,200 to 4,890,200 that coincided primarily with a single coding region of 705 amino acids with sequence similarity to *N. crassa* heterokaryon incompatibility gene *pin-c2* on the basis of BLAST analysis (5*e*-43) and containing a clearly defined HET domain (PF06985) (Kaneko *et al.* 2006). Analysis of the EP146 sequence contig corresponding to this region of Scaffold 3 revealed an ORF at the position of nucleotide polymorphism that encoded a 729-amino-acid ortholog of the EP155 protein with a conserved HET domain but high levels of amino acid polymorphism in the N-terminal and C-terminal flanking regions (53% overall identity) (Figure S5). These ORFs in strains EP155 and EP146 were designated candidate alleles *vic6-2* and *vic6-1*, respectively. The region of polymorphism extended upstream from *vic6* into the C-terminal portion (65% identity) of a small gene of 177 codons (Figure S6). The allelic forms of this small ORF were designated *pix6-2* and *pix6-1* (Figure 5, **p**artner of vics**ix**, based on functional analyses described below) in strains EP155 and EP146, respectively. Note that a high level of nucleotide identity is restored in the regions flanking the stretch of intense polymorphism associated with the candidate *vic6* locus.

vic7: The *vic7* locus was mapped 13.6 cM (~197,200 bp) from SSR marker CpSI006, which is located on Scaffold 6 at position 2,553,152 (Figure S7). Inspection of the EP155/EP146 sequence difference browser track revealed only two small (~200–300 bp) closely spaced regions of polymorphism located near positions 2,410,778 and 2,412,159, respectively (Figure 6). Neither region of polymorphism resided within an annotated ORF, but the first was adjacent to an ORF encoding a protein containing an ankyrin motif and the second was adjacent to a protein containing a HET motif. Further inspection determined that the ORF containing the HET domain extended in the C-terminal direction to give a predicted protein consisting of >600 amino acid residues. The corresponding alleles in strains EP155 and EP146 were 87% identical with a highly conserved HET domain and significant polymorphism limited primarily to the C-terminal domain (Figure S8). The different alleles of this candidate *vic* gene in strains EP155 and EP146 were designated *vic7-2* and *vic7-1*, respectively.

Association between polymorphism of candidate vic alleles and vic genotypes of C. parasitica field isolates

The polymorphisms associated with the putative *vic* loci provided the basis for PCR-based differentiation of the individual alleles for all candidate *vic* genes (primer information in Table S2). Allele specificity for the *vic4*, *vic6* (both *vic6* and *pix6*), and *vic7* loci was easily determined by the relative size of the allele-specific PCR products visualized in agarose gels (Figure S9) and confirmed by sequence analysis. Nucleotide sequence differences were used to distinguish the candidate *vic2-1* and *vic2-2* alleles and the adjacent sec9-like gene alleles *vic2a-1* and *vic2a-2* associated with the *vic2* locus. These PCR-based diagnostic tools were then used to compare the specificity of candidate *vic* allele with *vic* genotyping results for 26 field strains isolated from Finzel, Maryland (MD), Crevoladossala, Italy (VO), Bartow, West Virginia (BRU), and Depot Hill, New York (DU) (Milgroom and Cortesi 1999). As indicated in Table 2, complete concordance was observed between PCR-based *vic* allele specificity and *vic* tester strain-based genotyping for isolates from these four independent populations.

Disruption and functional analysis of candidate vic gene alleles

To define the functional role of the polymorphic *C. parasitica* candidate *vic* gene alleles in vegetative incompatibility, candidate *vic* alleles *vic2-2*, *vic6-2*, and *vic7-2* were disrupted

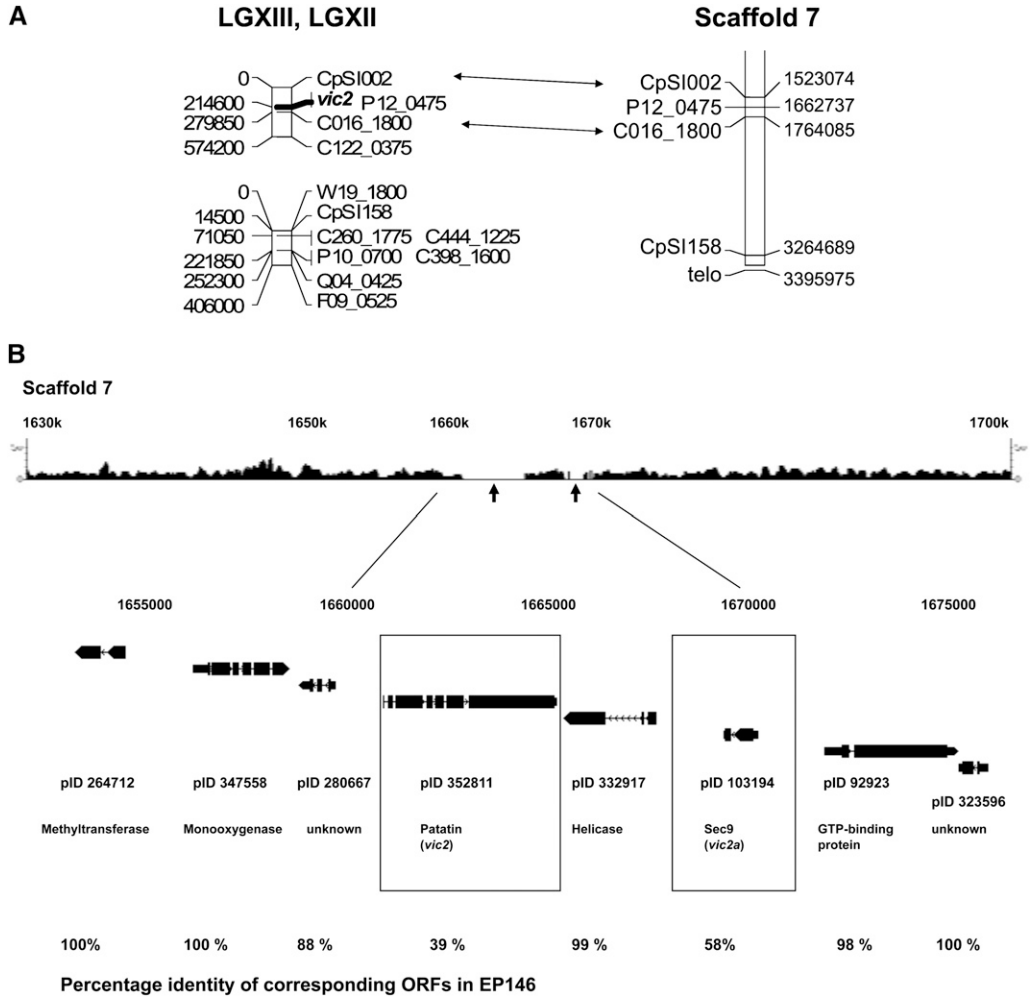

Figure 2 The candidate *vic2* locus. (A) Alignment of LGXII and LGXIII of the *C. parasitica* genetic linkage map generated by Kubisiak and Milgroom (2006), the latter of which contains the position of the *vic2* locus, with Scaffold 7 of version 2 of the *C. parasitica* genome sequence. The estimated physical distance (base pairs) of each marker from the end of the linkage group (shown on the left side of the linkage map) was calculated using the estimate of 1 cM = 14.5 kbp (Kubisiak and Milgroom 2006). Markers linking the physical and genetic maps are connected by double arrows. (B) The region of sequence polymorphism for *C. parasitica* strains EP155 and EP146 and machine-annotated ORFs located near the predicted *vic2* locus. The top track shows the density plot of the 454 sequence reads (scale indicated at both ends) that match a corresponding portion of Scaffold 7 of the EP155 reference genome sequence assembly. The 10-kbp region of polymorphism between the EP155 and EP146 genome sequences in the region mapped for the *vic2* locus is indicated by the absence of matching 454 sequence reads (arrows). The ORFs located within a 23-kbp region containing the polymorphic locus, with accompanying protein ID numbers, are shown below the 454 sequence read track. The candidate *vic2* genes *vic2-2* (patatin-like protein, pID 352811) and *vic2a-2* (sec9-like protein, pID103194) are indicated by boxes. The percentages of amino acid identity for the corresponding EP155 and EP146 ORFs are indicated at the bottom.

by transforming strain DK80, a mutant of the standard *C. parasitica* laboratory strain EP155 containing a disruption of the nonhomologous end-joining DNA repair pathway *ku80* gene homolog, to promote homologous recombination (Lan *et al.* 2008). Analysis of multiple independent disruption mutant strains for each candidate *vic* allele failed to find any obvious changes in growth, colony morphology, sporulation, or virulence (data not shown). Multiple selected disruption mutant strains for *vic2-2* (DK80 Δ*vic2-2*), *vic6-2* (DK80 Δ*vic6-2*), and *vic7-2* (DK80 Δ*vic7-2*) were subsequently examined for the effect of allele disruption on mycelial incompatibility, characterized by the formation of barrages or lines of demarcation (Powell 1995) and mycovirus transmission (Huber and Fulbright 1994; Cortesi *et al.* 2001). The candidate *vic4* allele was not disrupted because heteroallelism at the *vic4* locus, while associated with barrage formation, does not negatively affect virus transmission (Cortesi *et al.* 2001).

Mycelial incompatibility was not altered by disruption of candidate *vic2-2*, *vic6-2*, or *vic7-2* alleles. That is, barrage formation still occurred when these mutants were paired with the corresponding heteroallelic tester strains EU-6 (*2111-22*), EU-21 (*2211-12*), and EU-18 (*2211-21*), respectively (not shown).

The effect of disruption of *vic* allele candidates *vic2-2*, *vic6-2*, and *vic7-2* on virus transmission is presented in Table 3. Hypovirus transmission occurred successfully when EP155 and the derived DK80 strains were paired as either virus donor or virus recipient, showing that the deletion of the *ku80* gene homolog does not affect hypovirus transmission. Similar to previous reports (Cortesi *et al.* 2001), allelic differences at the *vic2* locus [DK80 (*2211-22*) *vs.* EU-6 (*2111-22*)] significantly reduced hypovirus transmission frequency to levels of 0/20–1/20 depending on whether the *vic2-2* allele is in the donor or the recipient strain, respectively. Disruption of the candidate *vic2-2* allele (patatin-like gene) in strain DK80 resulted in no significant increase in transmission when the mutant strain [DK80 Δ*vic2-2* (*2211-22*), where disruption is signified by a strike, *e.g.*, *2*] was the virus donor and EU-6 (*2111-22*) was the recipient, but resulted in 100% transmission when the mutant strain was the recipient.

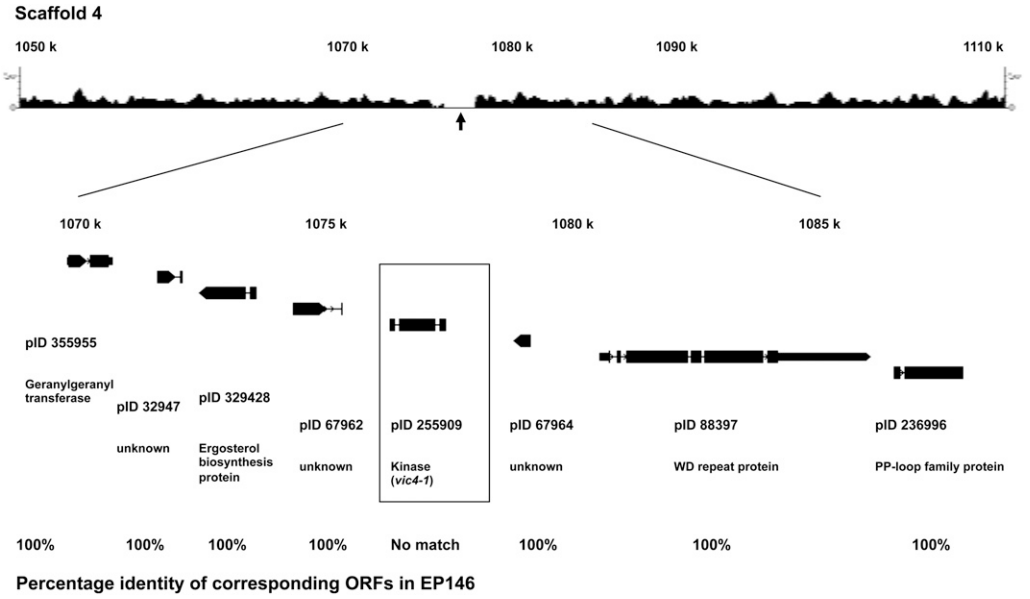

Figure 3 The candidate *vic4* locus: the region of sequence polymorphism for *C. parasitica* strains EP155 and EP146 and machine-annotated ORFs located near the predicted *vic4* locus. The ~2-kbp region of polymorphism between the EP155 and EP146 genome sequences in the region in Scaffold 4 mapped for the *vic4* locus (Figure S3) is indicated by the absence of 454 sequence reads generated from EP146 DNA that match the corresponding EP155 reference genome sequence (arrow). The open reading frames (ORFs) located within the 19-kbp region containing the polymorphic locus, with accompanying protein ID numbers and amino acid residue lengths, are shown below the 454 sequence read track. The boxed candidate *vic4* allele, *vic4-1* (pID 255909), in strain EP155 is absent in strain EP146, while other surrounding predicted proteins show perfect matches, as indicated at the bottom.

Similar results for virus transmission were observed for disruption of candidate *vic* allele *vic6-2*. In this case, allelic differences at the *vic6* locus [DK80 (*2211-22*) *vs.* EU-21 (*2211-12*)] resulted in a reduction in hypovirus transmission frequency to levels of 1/20 if the recipient strain contains the *vic6-1* allele and to 3/20 if the recipient strain contains the *vic2-2* allele. As observed for disruption of *vic2-2*, disruption of the candidate *vic6-2* allele resulted in no significant increase in virus transmission when the mutant strain was the donor, but resulted in 100% transmission when the mutant strain was the virus recipient.

As reported by Cortesi *et al.* (2001) and observed in Table 3, strains heteroallelic at the *vic7* locus [DK80 (*2211-22*) *vs.* EU-18 (*2211-21*)] exhibit an asymmetric virus transmission pattern with 100% transmission occurring when the recipient contained the *vic7-2* allele and much lower transmission occurring when the recipient contained *vic7-1*. Since virus transmission to a *vic7-2*–containing strain of a *vic7* heteroallelic pair is already 100%, disruption of the candidate *vic7-2* allele cannot increase acceptance of virus. However, there was a significant increase in virus transmission frequency from 2/20 to 9/20 (Table 3) when the *vic7-2* mutant strain served as the virus donor.

The increased frequency of virus transmission observed for *vic2-2* and *vic6-2* mutant strains when serving as a recipient and the *vic7-2* mutant when serving as the virus donor

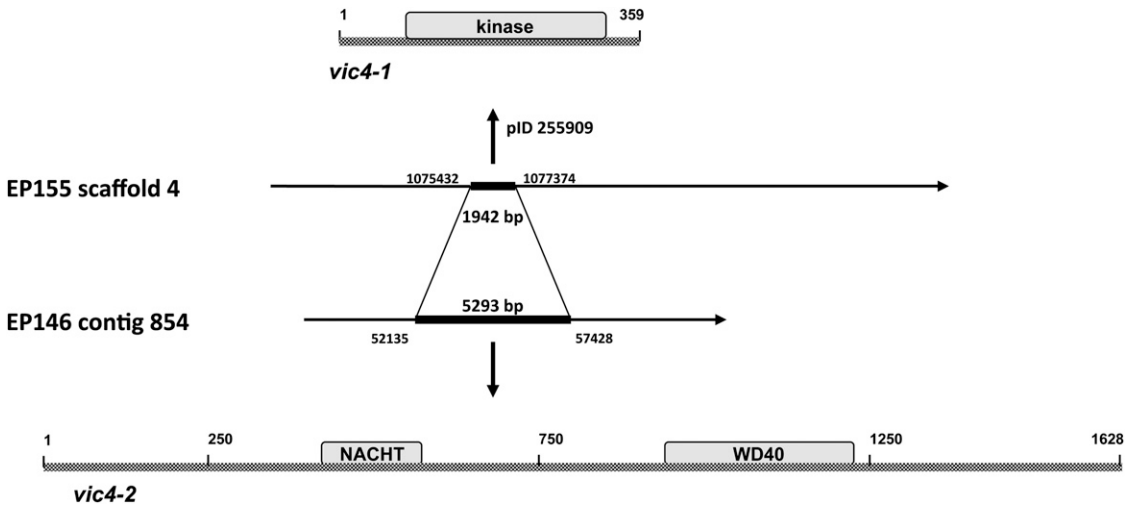

Figure 4 The candidate *vic4-1* allele in EP155, which contains a fructosamine kinase/phosphotransferase enzyme family domain, is replaced by an unrelated ORF of 1628 amino acids in length in the corresponding EP146 sequence. This candidate *vic4-2* allele contains NACHT and WD40 motifs reported for *het* genes from *P. anserina* (reviewed in Paoletti and Saupe 2009).

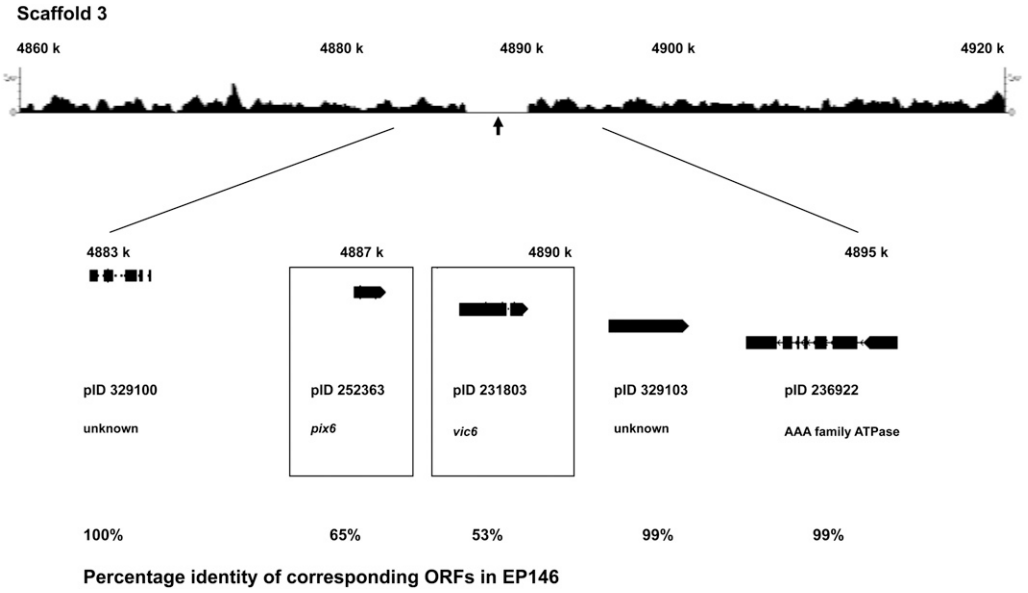

Figure 5 The candidate *vic6* locus: the region of sequence polymorphism for *C. parasitica* strains EP155 and EP146 and machine-annotated ORFs located near the predicted *vic6* locus (Figure S4). The ~3.7-kbp region of polymorphism between the EP155 and EP146 genome sequences on Scaffold 3 in the region mapped for the *vic6* locus is indicated by the absence of 454 sequence reads generated from EP146 DNA that match the corresponding EP155 reference genome sequence (arrow). The ORFs located within a 13.4-kbp region containing the polymorphic locus, with accompanying protein ID numbers, are shown below the 454 sequence read track. The boxed candidate *vic6* gene (pID 231803), which contains a HET domain, and adjacent ORF *pix6* (pID 252363) showed a greater degree of sequence polymorphism than surrounding ORFs, which showed near perfect matches.

strain is consistent with a role for these candidate *vic* alleles in vegetative incompatibility, even though barrage formation is still observed. This raised the question of whether disruption of both candidate *vic* alleles of a heteroallelic pair would abolish barrage formation and eliminate the barrier to virus transmission.

Disruption of vic6-2 and vic6-1

The candidate *vic6-1* allele was disrupted in tester strain EU-21(*2211-12*) that differs in *vic* alleles from the DK80 strain only at the *vic6* locus (Cortesi and Milgroom 1998). Disruption of either the candidate *vic6-1* or the *vic6-2* alleles independently resulted in no change in mycelial incompatibility (Figure 7). The DK80 Δ*vic6-2* mutants formed barrages when paired with the EU-21 tester strain and retained compatibility with the DK80 parent strain and EP155 (see above), while the EU-21 Δ*vic6-1* mutants formed barrages when paired with EP155 or DK80 and were compatible with the EU-21 parent strain (results not shown). However, barrage formation was abolished when the two mutant strains were paired (Figure 7). Additionally, the frequency of virus transmission increases to 100% when the *vic6* alleles are disrupted in both

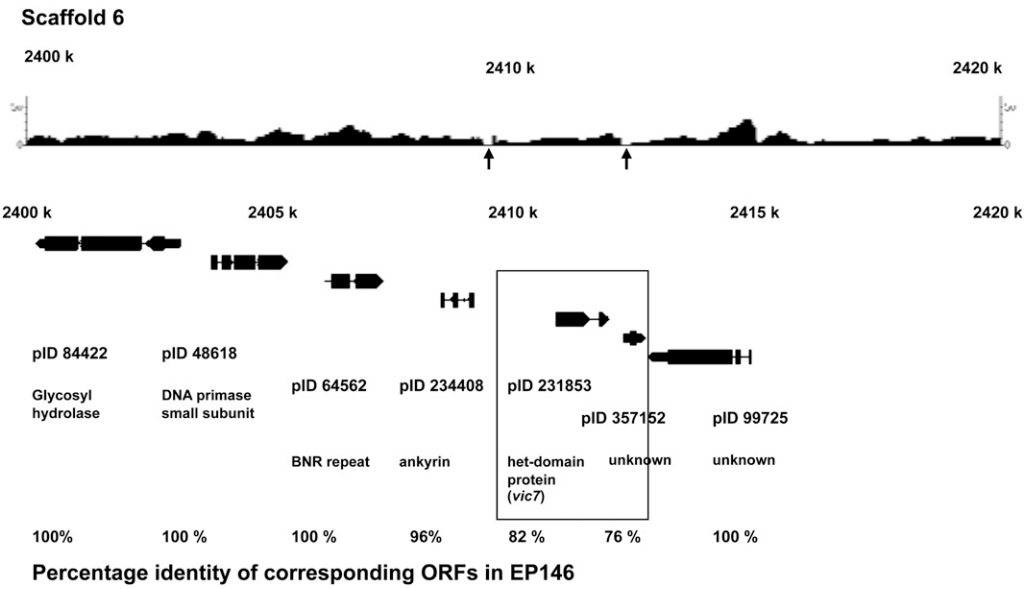

Figure 6 The candidate *vic7* locus: the region of sequence polymorphism for *C. parasitica* strains EP155 and EP146 and machine-annotated ORFs located near the predicted *vic7* locus. Polymorphisms between the EP155 and EP146 genome sequences on Scaffold 6 in the region mapped for the *vic7* locus (Figure S7) are indicated by the absence of 454 sequence reads generated from EP146 DNA that match the corresponding EP155 reference genome sequence (arrows). The ORFs located within a 20-kbp region containing the polymorphic locus, with accompanying protein ID numbers, are shown below the 454 sequence read track. The two boxed EP155 ORFs, pID 231853 and pID 357152, showed a greater degree of sequence divergence than the surrounding ORFs, which showed near perfect or perfect matches. When manually annotated, these two ORFs became one HET domain-containing ORF corresponding to candidate *vic7* allele *vic7-2*. The percentages of amino acid identity for the corresponding EP155 and EP146 ORFs surrounding the putative *vic7* locus are indicated at the bottom.

Table 2 Correspondence between barrage-based *vic* genotype and PCR-based *vic* genotype in *C. parasitica* field isolates

		vic2 locus		*vic4*	*vic6* locus		*vic7*
Isolate[a]	Genotype	*vic2(ptn)*[b]	*vic2a(sec9)*[b]	*vic4*[c]	*vic6*[c]	*pix6*[c]	*vic7*[c]
EP155	*2211-22*	2	2	1	2	2	2
EP146	*2112-11*	1	1	2	1	1	1
MD3	*2112-11*	1	1	2	1	1	1
MD8	*2212-12*	2	2	2	1	1	2
MD11	*2121-11*	1	1	1	1	1	1
MD16	*1212-22*	2	2	2	2	2	2
MD18	*2211-11*	2	2	1	1	1	1
MD19	*1122-11*	1	1	2	1	1	1
MD22	*2112-12*	1	1	2	1	1	2
MD28	*1212-11*	2	2	2	1	1	1
MD33	*2211-22*	2	2	1	2	2	2
MD46	*2122-11*	1	1	2	1	1	1
MD52	*1211-12*	2	2	1	1	1	2
MD55	*1112-21*	1	1	2	2	2	1
VO1	*2112-22*	1	1	2	2	2	2
VO21	*2111-22*	1	1	1	2	2	2
VO59	*2111-11*	1	1	1	1	1	1
BRU2	*2212-21*	2	2	2	2	2	1
BRU10	*2222-12*	2	2	2	1	1	2
BRU16	*2212-22*	2	2	2	2	2	2
BRU17	*2112-21*	1	1	2	2	2	1
BRU19	*2211-11*	2	2	1	1	1	1
BRU69	*1211-11*	2	2	1	1	1	1
DU14	*1212-11*	2	2	2	1	1	1
DU29	*2212-22*	2	2	2	2	2	2
DU63	*2111-11*	1	1	1	1	1	1
DU72	*2121-11*	1	1	1	1	1	1
DU74	*2211-12*	2	2	1	1	1	2

vic genotypes are abbreviated as the alleles at each of six known *vic* loci, as defined in Table 1. The PCR products for *vic2(ptn)* and *vic2a(sec9)* are both associated with the *vic2* locus while the PCR products for *vic6* and *pix6* are both associated with the *vic6* locus. PCR-based markers are not yet available for *vic1* or *vic3*.

[a] MD isolates are from Finzel, Maryland; VO isolates are from Crevoladossola, Italy; BRU isolates are from Bartow, West Virginia; DU isolates are from Depot Hill, New York. These isolates were used in a previous population study (Milgroom and Cortesi 1999).

[b] *vic2* candidates *vic2* patatin-like protein (*ptn*) and *vic2a* Sec9-like protein (*sec9*): PCR products were directly sequenced to assign allele 1 or 2.

[c] *vic4*, *vic6*, *pix6*, and *vic7*: alleles assigned on the basis of the PCR product size. In addition, for all MD isolates, *vic6* and *vic7* PCR products were sequenced along with several isolates from the rest of the list.

DK80 and EU-21 irrespective of which mutant strain is donor or recipient (Table 3). Thus, both barrage formation and restrictions to virus transmission were eliminated when both alleles were disrupted.

We next tested whether *vic6* disruption mutant strains could form stable heterokaryons using methods described previously (Smith *et al.* 2006). Heterokaryon formation results in rapidly growing sectors on double-antibiotic medium when each individual strain carries resistance to only one antibiotic. In this study, we used PDA containing hygromycin and G418 (PDA+hyg+G418) as the double-selection medium. As indicated in Table 4, heterokaryotic outgrowths were observed with strain pairs that had identical alleles at all six *vic* loci, *e.g.*, DK80hygR and DK80neoR. Upon transfer of hyphae from these outgrowths to fresh (PDA+hyg+G418) medium, a sustained radial growth rate of between 6.5 and 8.0 mm per day was observed. Outgrowths were not observed for the *vic6* heteroallelic pairs [DK80neoR (*2211-22*) + EU-21hygR (*2211-12*)] or [DK80hygR (*2211-22*) + EU-21neoR (*2211-12*)] or for heteroallelic pairs deleted in either *vic6-1* or *vic6-2* alone. In contrast, heterokaryotic sectors did develop for the pairing of EU-21 Δ*vic6-1* (*2211-12*) and DK80 Δ*vic6-2* (*2211-22*) that have their respective allelic forms (*vic6-1* and *vic6-2*) disrupted. Hyphal transfers from the [DK80 Δ*vic6-2* + EU-21 Δ*vic6-1*] outgrowths to PDA+hyg+G418 medium grew equivalently to compatible heterokaryons (7.4 ± 0.4 mm per day, SE, $n = 5$) and significantly faster than transfers from *vic6*-incompatible pairings (<0.3 mm per day). Thus, stable heterokaryon formation is possible only when both *vic6* gene allelic forms are deleted in the paired strains. This confirms a role for the candidate polymorphic *vic6* alleles as determinants of vegetative incompatibility.

Evidence for nonallelic interactions at the vic6 locus

It was of interest to test whether the *vic6* alleles could functionally replace each other. To this end, the disrupted *vic6* allele in mutant strain DK80 Δ*vic6-2* was replaced with an intact *vic6-1* allele from strain EP146 linked to a neomycin resistance gene. Examination of DK80 Δ*vic6-1* replacement strains revealed abnormal growth characteristics and colony morphology (Figure S10) that included reduced aerial hyphae, reduced biomass production, irregular margins, and reduced conidiation. The association of abnormal phenotypic changes with the replacement of the disrupted *vic6-2* allele with an intact *vic6-1* allele suggested the possibility of functional interactions between the *vic6-1* product and a gene product other than that encoded by *vic6-2*.

As indicated in Figure 5, the candidate *vic6* locus also contains a small polymorphic ORF, *pix6*, adjacent to the candidate *vic6* gene. The two *pix6* alleles were found to be in linkage disequilibrium with the corresponding *vic6* alleles in the natural *C. parasitica* populations examined (Table 2), consistent with a functional association, because repeated recombination in nature is likely to have eroded this complete association even though the two loci are tightly linked. Independent disruption of *pix6-2* in strain DK80 or *pix6-1* in strain EU-21 did not eliminate barrage formation (Table 5, pairings E and F). However, the *pix6-2* and *pix6-1* disruption mutant strains were found to very efficiently promote hypovirus transmission (100%) when serving as the donor, but exhibited no increase when serving as a recipient (Table 5). Importantly, this is completely opposite to the properties of the *vic6* disruption mutant strains that promoted virus transmission only when serving as the recipient strain (summarized in Table 5, pairings B and C).

As observed when pairing disruption mutant Δ*vic6-1* and Δ*vic6-2* strains (Tables 3 and 5, pairing D), the paired Δ*pix6-1* and Δ*pix6-2* mutant strains failed to form barrages and exhibited no resistance to virus transmission (Table 5, pairing G). Thus, potential allelic interactions either between *vic6-1* and *vic6-2* (pairing G) or between *pix6-1* and *pix6-2*

Table 3 Hypovirus transmission frequency for disruption mutants of candidate *vic* alleles at *vic2*, *vic6*, and *vic7*

Donor	Recipient	Transmission	*P*-value[a]
DK80 (*2211-22*)	EP155 (*2211-22*)	20/20	
EP155 (*2211-22*)	DK80 (*2211-22*)	20/20	
DK80 (*2211-22*)	EU-6 (*2111-22*)	0/20	0.245
DK80 Δ*vic2-2* (*22~~1~~11-22*)	EU-6 (*2111-22*)	2/20	
EU-6 (*2111-22*)	DK80 (*2211-22*)	1/20	<0.001
EU-6 (*2111-22*)	DK80 Δ*vic2-2* (*22~~1~~11-22*)	20/20	
DK80 (*2211-22*)	EU-21 (*2211-12*)	1/20	0.171
DK80 Δ*vic6-2* (*2211-~~2~~2*)	EU-21 (*2211-12*)	4/20	
EU-21 (*2211-12*)	DK80 (*2211-22*)	3/20	<0.001
EU-21 (*2211-12*)	DK80 Δ*vic6-2* (*2211-~~2~~2*)	20/20	
DK80 (*2211-22*)	EU-18 (*2211-21*)	2/20	0.015
DK80 Δ*vic7-2* (*2211-22~~1~~*)	EU-18 (*2211-21*)	9/20	
EU-18 (*2211-21*)	DK80 (*2211-22*)	20/20	ND
EU-18 (*2211-21*)	DK80 Δ*vic7-2* (*2211-22~~1~~*)	20/20	
DK80 Δ*vic6-2* (*2211-~~2~~2*)[b]	EU-21 (*2211-12*)	4/20	<0.001
DK80 Δ*vic6-2* (*2211-~~2~~2*)	EU-21 Δ*vic6-1* (*2211-~~1~~2*)	20/20	
EU-21 (*2211-12*)[b]	DK80 (*2211-22*)	3/20	<0.001
EU-21 Δ*vic6-1* (*2211-~~1~~2*)	DK80 Δ*vic6-2* (*2211-~~2~~2*)	20/20	

[a] *P*-values for Fisher's exact tests comparing the frequency of virus transmission when a *vic* allele in one isolate is disrupted. ND, not determined.
[b] Repeated from above for comparison with double-allele disruption mutant parings.

(pairing D) alone are insufficient to cause barrage formation or restrict virus transmission (100% transmission in both directions). In contrast, barrage formation was observed for all paired mutant strains in which one of the two possible nonallelic interactions between *pix6* and *vic6* alleles remained intact (Table 5, pairings B, C, E, and F). Moreover, elimination of both potential allelic interactions and one, but not both, possible *pix6-vix6* nonallelic interaction by disruption of *pix6-2* and *vic6-1* or *pix6-1* and *vic6-2* alleles still allowed barrage formation but resulted in an asymmetric, allele-specific, loss of resistance to virus transmission (Table 5, pairings H and I). Virus transmission was unrestricted from the DK80 Δ*pix6-2 vic6-2* strain into the EU-21 *pix6-1* Δ*vic6-1* strain (pairing H), but was restricted in this pairing when the EU-21–derived strain was the virus donor. The reciprocal situation was observed in pairing I: virus transmission was restricted from DK80 *pix6-2* Δ*vix6-2* into EU-21 Δ*pix6-1 vic6-1* but was unimpeded in the opposite direction. Importantly, disruption of *pix6-2* and *vic6-2* in the same strain (Table 5, paring J) eliminated barrage formation (Figure S11) as well as resistance to virus transmission in both directions (Table 5).

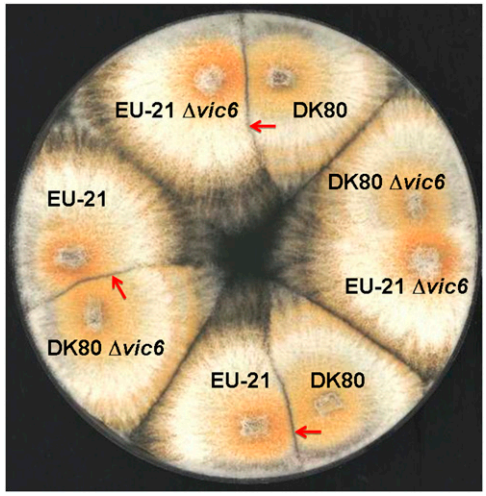

Figure 7 Mycelial incompatibility assay for strains disrupted in candidate *vic* alleles *vic6-1* and *vic6-2* in incompatible isolates DK80 (*2211-22*) and tester strain EU-21 (*2211-12*) (barrage lines indicated by red arrows). Barrage formation resulting from an incompatible interaction occurred when *vic6-1* disruption mutants [EU-21 Δ*vic6-1* (*2211-~~1~~2*)] were paired with strain DK80 as shown at the top or when *vic6-2* disruption mutants [DK80 Δ*vic6-2* (*2211-~~2~~2*)] were paired with tester strain EU-21 as shown at the left. In contrast, barrage formation was abolished when both mutants were paired as shown at the right [DK80 Δ*vic6-2* (*2211-~~2~~2*) *vs.* EU-21 Δ*vic6-1* (*2211-~~1~~2*)].

The combined results provide strong evidence that vegetative incompatibility for strains heteroallelic at the *vic6* locus requires nonallelic rather than allelic interactions between two tightly linked genes, *pix6* and *vic6*. Nonallelic interactions involving both sets of *pix6* and *vic6* alleles are required for a robust incompatibility reaction that severely restricts two-way virus transmission. Disruption of one of the two nonallelic interactions weakens the incompatibility reaction as indicated by enhanced virus transmission. Moreover, the asymmetric, gene-specific nature of the resulting enhancement in virus transmission suggests an element of mechanistic directionality underlying the incompatible reaction.

Discussion

The *C. parasitica* vegetative incompatibility system has been the subject of considerable interest for >3 decades due to its reported role in limiting virus transmission and consequently, the effectiveness of virus-mediated control of chestnut blight (Van Alfen *et al.* 1975; Anagnostakis 1982a; Nuss 1992; MacDonald and Fulbright 1991; Heiniger and Rigling 1994; Milgroom and Cortesi 2004). Using a comparative

Table 4 Heterokaryon compatible (+) and incompatible (−) pairings with mean growth rates in parentheses (millimeters per day)

	hyg^R strains			
	Dk80hygR (*2211-22*)	EU-21hygR (*2211-12*)	DK80 Δ*vic6-2* (*2211-22*)	DK80 Δ*vic7-2* (*2211-22*)
neo^R strains				
DK80neoR	+	−	+	+
(*2211-22*)	(8.0)	(<0.1)	(6.7)	(6.6)
EU-21neoR	−	+	−	−
(*2211-12*)	(<0.3)	(7.6)	(<0.1)	(<0.1)
EU-21 Δ*vic6-1*	−	+	+	−
(*2211-12*)	(<0.3)	(6.7)	(7.0)	(<0.2)

genomics approach, we report here the identification of a total of seven candidate incompatibility genes associated with four *C. parasitica vic* loci. Subsequent functional analysis confirmed that candidate genes at the *vic2*, *vic6*, and *vic7* loci do contribute to restriction of virus transmission. These studies provide molecular and functional confirmation for a role of the *vic* loci in regulating virus transmission, based previously on genetic evidence only. Detailed analysis of the candidate *vic6* locus revealed a gene complex consisting of two tightly linked but distinct genes and provided evidence for the contribution of nonallelic interactions to the restrictions placed by the *C. parasitica* vegetative incompatibility system on mycovirus transmission.

The approach used to identify the candidate *vic* genes took advantage of the general polymorphic nature of nonself recognition genes (reviewed in Richman 2000). It also relied on the collection of 64 *vic* tester strains (Cortesi and Milgroom 1998) to determine the differences in *vic* genotypes for the reference and resequenced strains. Additionally, it was guided by the predicted positions of the *vic* loci on a genetic linkage map (Kubisiak and Milgroom 2006; Kubisiak *et al.* 2007) and corresponding genome sequence assembly (Department of Energy/Joint Genome Institute and *Cryphonectria* genome consortium, unpublished results). Reliance on the presence of HET domains (PF06985) associated with the majority of *het* gene complexes in *N. crassa* and *P. anserina* alone for identification of *C. parasitica vic* genes was not an option. Blast analysis with the HET domain gave 96 hits in the *C. parasitica* genome assembly (our unpublished results). This compares with 120 HET domains for *P. anserina* (Paoletti *et al.* 2007), 55 for *N. crassa*, and 38 for *Aspergillus oryzae* (Fedorova *et al.* 2005). Moreover, neither the *vic2* nor the *vic4* gene candidates were found to contain HET domains.

The complete correspondence between the results of PCR-based *vic* allele specificity and *vic*-tester strain-aided

Table 5 Summary of effects of gene disruption in the *vic6* locus on barrage formation and hypovirus transmission

				Virus movement[a]	
Pairing	Strains	Genotype	Barrage	% (2 to 1)	% (1 to 2)
A	DK80	*pix6-2*, *vic6-2*	Yes	5 (1/20)	15 (3/20)
	EU-21	*pix6-1*, *vic6-1*			
B	DK80 Δ*vic6*[b]	*pix6-2*, **Δ*vic6-2***	Yes	15 (6/40)	100 (30/30)
	EU-21	*pix6-1*, *vic6-1*			
C	DK80	*pix6-2*, *vic6-2*	Yes	100 (20/20)	17 (5/30)
	EU-21 Δ*vic6*	*pix6-1*, **Δ*vic6-1***			
D	DK80 Δ*vic6*	*pix6-2*, **Δ*vic6-2***	No	100 (20/20)	100 (20/20)
	EU-21 Δ*vic6*	*pix6-1*, **Δ*vic6-1***			
E	DK80 Δ*pix6*	**Δ*pix6-2***, *vic6-2*	Yes	100 (32/32)	0 (0/30)
	EU-21	*pix6-1*, *vic6-1*			
F	DK80	*pix6-2*, *vic6-2*	Yes	7 (2/30)	100 (20/20)
	EU-21 Δ*pix6*	**Δ*pix6-1***, *vic6-1*			
G	DK80 Δ*pix6*	**Δ*pix6-2***, *vic6-2*	No	100 (20/20)	100 (20/20)
	EU-21 Δ*pix6*	**Δ*pix6-1***, *vic6-1*			
H	DK80 Δ*pix6*	**Δ*pix6-2***, *vic6-2*	Yes	100 (32/32)	10 (3/30)
	EU-21 Δ*vic6*	*pix6-1*, **Δ*vic6-1***			
I	DK80 Δ*vic6*	*pix6-2*, **Δ*vic6-2***	Yes	13 (4/30)	100 (20/20)
	EU-21 Δ*pix6*	**Δ*pix6-1***, *vic6-1*			
J	DK80 Δ*pix6*Δ*vic6*	**Δ*pix6-2***, **Δ*vic6-2***	No	100 (20/20)	100 (20/20)
	EU-21	*pix6-1*, *vic6-1*			

[a] "2 to 1" means virus transmission from a strain with a *vic6-2* genotype, *e.g.*, DK80, to a strain with a *vic6-1* genotype, *e.g.*, EU-21. The inverse holds for "1 to 2". Transmission data are reported as percentage of independent trials, with numbers in parentheses showing the number of successes over the number of trials.

[b] All *pix6-1* and *vic6-1* gene disruption mutants were made in the strain EU-21 background. All *pix-2* and *vic6-2* disruption mutants were made in the strain DK80 background. Disrupted alleles are indicated in bold.

genotyping for 26 *C. parasitica* field isolates (Table 3) provides strong correlative evidence linking the polymorphic candidate *vic* alleles with the *vic* system. The strains tested to date represent the two sequenced laboratory strains and field isolates from three independent North American populations and one European population. The field isolates are valuable for establishing an association between the vegetative incompatibility phenotype and specific alleles because they are derived from natural populations in which repeated recombination would have broken down linkage disequilibrium that might have resulted from spurious correlations in laboratory strains. Analysis of the amplified and sequenced PCR fragments identified only two alleles per locus and no evidence for additional alleles. A much wider survey of allelic diversity in field isolates is warranted, including in isolates from Japan and China, where *C. parasitica* is native and from where it was introduced into North America and Europe, causing devastating chestnut blight epidemics (reviewed in Milgroom and Cortesi 2004). Analysis of *vic* allele sequences would allow a determination of whether they are under positive selection and polymorphism is maintained by balancing selection, as found for *N. crassa* and *P. anserina* (Saupe *et al.* 1995; Wu *et al.* 1998; Micali and Smith 2006; Chevanne *et al.* 2010; Hall *et al.* 2010). The PCR-based test for *vic* allele specificity also provides a valuable tool for determining the *vic* diversity profiles of *C. parasitica* forest and orchard populations. The molecular identification of *vic* alleles opens new approaches for constructing a more complete picture of the influence of *vic* diversity on hypovirus transmission at the population level and a better understanding of how mycoviruses influence the evolution of the *vic* system.

A functional role in the restriction of virus transmission was demonstrated for three of the candidate *vic* genes through gene disruption analysis. Disruption of the candidate *vic2* allele encoding the patatin-like protein resulted in a dramatic increase in virus transmission from 5 to 100% when the mutant strain served as the recipient, but resulted in little change if the mutant served as the donor (Table 3). A similar dramatic asymmetric effect on virus transmission was observed when the *vic6* disruption mutant served as a recipient in virus transmission assays (Table 3). Analysis of the HET domain-containing candidate *vic7* gene was complicated by the fact that virus transmission is not inhibited when the recipient strain has the *vic7-2* allele. Consequently, disruption of this allele present in the DK80 strain would not result in any increase. However, the trend toward higher transmission rates (from 2/20 to 9/20) observed when the mutant strain served as the donor is consistent with a contribution of the candidate *vic7* to restriction of virus transmission.

The fact that the increase in virus transmission observed for the *vic* mutant strains was not accompanied by a loss of barrage formation was initially surprising. However, our results reinforce previous observations that heteroallelism at the *vic4* locus results in barrage formation but does not prevent heterokaryon formation (Smith *et al.* 2006) or, more importantly for this study, does not restrict hypovirus transmission (Cortesi *et al.* 2001); *i.e.*, barrage formation and restriction of virus transmission are not necessarily tightly coupled. One interpretation is that disruption of one of the alleles for a heteroallelic pair retards PCD to an extent that virus transmission is increased, especially when the mutant serves as the recipient strain, but not to an extent that barrage formation is prevented. A slight delay in the initiation of PCD following fusion of the donor and recipient hyphae would increase the frequency with which virus can escape into adjacent recipient cells and then move unrestricted through the recipient mycelium, infecting the mycelium in the growing margin of the colony (Biella *et al.* 2002).

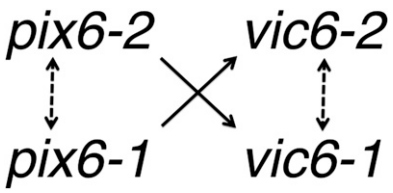

Figure 8 Model for interactions between the linked genes *pix6* and *vic6* at the *vic6* locus. Nonallelic interactions supported by data summarized in Table 5 are indicated by solid arrows. Arrow direction reflects how the *pix6* gene product potentially acts in *trans* with the *cis*-acting *vic6* gene product to effect asymmetric virus transmission. No evidence was obtained in this study for potential allelic interactions (dashed double arrows).

Genetic mechanisms of vegetative incompatibility can be placed into two categories. First, *allelic* interactions are triggered by interplay between different alleles of a single incompatibility gene. Second, *nonallelic* interactions involve different linked or unlinked incompatibility genes. Examples of nonallelic incompatibility gene pairs include *un-24/het-6* and *het-c/pin-c* in *N. crassa* (review in Dementhon *et al.* 2006) and *het-c/het-e* and *het-c/het-d* in *P. anserina* (review in Saupe 2000).

Strong evidence for nonallelic interactions was obtained for the two polymorphic genes, *pix6* and *vic6*, contained within the candidate *vic6* locus. As indicated in Figure 8, pairing of strains heteroallelic at the *vic6* locus can result in a limited set of possible interactions between these tightly linked genes that include two allelic interactions (*pix6-1* with *pix6-2* and *vic6-1* with *vic6-2*) and two nonallelic interactions (*pix6-1* with *vic6-2* and *pix6-2* with *vic6-1*). Since mutant strain DK80 Δ*pix6-2 vic6-2* was compatible with strain EU-21 Δ*pix6-1 vic6-1* and strain DK80 *pix6-2* Δ*vic6-2* was compatible with strain EU-21 *pix6-1* Δ*vic6-1*, it is clear that the potential *pix6* or *vic6* allelic interactions alone are insufficient to cause barrage formation (Figure 8 and summarized in Table 5).

Elimination of the potential *vic6* allelic interaction and either of the two possible *pix6–vic6* nonallelic interactions by disruption of a single *vic6* allele allowed barrage formation but resulted in asymmetric loss of resistance to virus transmission by the Δ*vic6* strain (Table 5, pairings B and C).

In contrast, elimination of the potential *pix6* allelic interaction and either of the two *pix6–vic6* nonallelic interactions by disruption of a single *pix6* allele allowed barrage formation but resulted in asymmetric decreased resistance to virus transmission by the strain that has *vic6* intact (Table 5, parings E and F). This pattern of barrage formation but asymmetric enhancement of virus transmission holds when Δ*pix6* and Δ*vic6* mutant strains were paired (Table 5, pairings H and I), in which case both potential allelic interactions and one potential nonallelic interaction are eliminated. Thus, barrage formation was observed for every mutant pairing in which one of the possible nonallelic interactions remained intact. However, the strength of the incompatible reaction was decreased when one nonallelic interaction was disrupted, as witnessed by enhanced virus transmission.

The observation that a strain with *pix6* disrupted has enhanced virus donor capability while a strain disrupted at *vic6* is more susceptible to virus infection is intriguing. It will be interesting to determine whether this gene-dependent asymmetry in enhanced virus transmission correlates with asymmetric delay in PCD for the two interacting strains and whether the asymmetry is dependent on the presence of virus. It is conceivable that the *pix6* gene product is mobile and acts in *trans* to trigger PCD initially or preferentially by interacting with the gene product of an anchored, *cis*-acting incompatible gene product of *vic6*. For example, disruption of the *pix6-1* allele, the corresponding *vic6-2* allele, or both would then result in an asymmetric delay in PCD in the *vic6-2*–containing strain, leading to the opportunity for increased virus transmission early on in the interaction, without eliminating eventual PCD, heterokaryon incompatibility, and barrage formation. Under this scenario, a similar situation would hold for disruption of the *pix6-2* and/or *vic6-1* alleles.

Multiple polymorphic genes were also identified at the candidate *vic2* and *vic7* loci, raising the possibility for nonallelic interactions at these loci as well. For example, nonallelic interactions parallel to those observed for the *vic6* and *pix6* alleles could be envisioned for the closely linked *vic2* and *vic2a* alleles. Future studies will focus on the physical interactions, cellular distribution, and movement of candidate *vic* gene products to provide a mechanistic understanding of how these interactions drive PCD and resistance to virus transmission. Strategies that disrupt all or most allelic and nonallelic interactions would be expected to enhance hypovirus spread and biological control potential.

An inducible RNA silencing surveillance system was recently shown to serve as a cellular antiviral defense response in *C. parasitica* to target hypovirus RNA for degradation (Segers *et al.* 2007; Zhang *et al.* 2008; Sun *et al.* 2009b). Hypoviruses, in turn, encode a suppressor of RNA silencing, p29. Hypovirus mutants that lack p29 accumulate to a much lower level in infected mycelia, resulting in a reduced level of virus transmission through asexual spores (Suzuki *et al.* 2003). That is, p29 is able to promote virus transmission by suppressing the cellular RNA silencing antiviral defense response. Thus, the RNA silencing surveillance system and the *vic* genetic system could be viewed as having evolved as complementary cellular and population-level antiviral defense mechanisms. Interestingly, Biella *et al.* (2002) reported that hypovirus infection influences the frequency of *vic*-associated programmed cell death, with an additional potential mechanism for promoting its own transmission. This raises the possibility of a mechanistic link between the interactions of hypoviruses with the two principal antiviral defense strategies of vegetative incompatibility and RNA silencing.

Acknowledgments

The authors thank Haofeng Chen and Peter Houde of the New Mexico State University Genome Sequencing Laboratory for technical assistance. Thomas Kubisiak, U.S. Department of Agriculture Forest Service, Southern Research Station, Southern Institute of Forest Genetics, Saucier, Mississippi, made major contributions to assembly of *C. parasitica* genome sequence scaffolds and the alignment of linkage group markers with the scaffolds. This work was supported by National Science Foundation awards DBA-0821806 (to P. Houde), MCB-1051453 (to A.L.D.), and MCB-1051331 (to D.L.N.). The authors declare that they have no conflict of interest.

Literature Cited

Anagnostakis, S. L., 1982a Biological control of chestnut blight. Science 215: 466–471.

Anagnotakis, S. L., 1982b Genetic analysis of *Endothia parasitica*: linkage map of four single genes and three vegetative compatibility types. Genetics 102: 25–28.

Anagnostakis, S. L., B. Hau, and J. Kranz, 1986 Diversity of vegetative compatibility groups of *Cryphonectria parasitica* in Connecticut and Europe. Plant Dis. 70: 536–538.

Andrews, D., B. Beames, M. D. Summers, and W. D. Park, 1988 Characterization of the lipid acyl hydrolase activity of the major potato (Solanum tuberosum) tuber protein, patatin, by cloning and abundant expression in a baculovirus vector. Biochem. J. 252: 199–206.

Biella, S., M. L. Smith, J. R. Aist, P. Cortesi, and M. G. Milgroom, 2002 Programmed cell death correlates with virus transmission in a filamentous fungus. Proc. Biol. Sci. 269: 2269–2276.

Caten, C. E., 1972 Vegetative incompatibility and cytoplasmic infection in fungi. J. Gen. Microbiol. 72: 221–229.

Chevanne, D., S. J. Saupe, C. Clave, and M. Paoletti, 2010 WD-repeat instability and diversification of the *Podospora anserina* hnwd non-self recognition gene family. BMC Evol. Biol. 10: 134–146.

Chen, B., G. H. Choi, and D. L. Nuss, 1993 Mitotic stability and nuclear inheritance of integrated viral cDNA in engineered hypovirulent strains of the chestnut blight fungus. EMBO J. 12: 2991–2998.

Chen, B., G. H. Choi, and D. L. Nuss, 1994 Attenuation of fungal virulence by synthetic infectious hypovirus transcripts. Science 264: 1762–1764.

Churchill, A. C. L., L. M. Ciufetti, D. R. Hansen, H. D. Van Etten, and N. K. Van Alfen, 1990 Transformation of the fungal pathogen *Cryphonectria parasitica* with a variety of heterologous plasmids. Curr. Genet. 17: 25–31.

Cortesi, P., and M. G. Milgroom, 1998 Genetics of vegetative incompatibility in *Cryphonectria parasitica*. Appl. Environ. Microbiol. 64: 2988–2994.

Cortesi, P., C. E. McCulloch, H. Song, H. Lin, and M. G. Milgroom, 2001 Genetic control of horizontal virus transmission in the chestnut blight fungus, *Cryphonectria parasitica*. Genetics 159: 107–118.

Dementhon, K., G. Iyer, and N. L. Glass, 2006 VIB-1 is required for expression of genes necessary for programmed cell death in *Neurospora crassa*. Eukaryot. Cell 5: 2161–2173.

Fedorova, N. D., J. H. Badger, G. D. Robson, J. R. Wortman, and W. C. Nierman, 2005 Comparative analysis of programmed cell death pathways in filamentous fungi. BMC Genomics 6: 177.

Ghabrial, S. A., and N. Suzuki, 2009 Viruses of plant pathogenic fungi. Annu. Rev. Phytopathol. 47: 353–384.

Glass, N. L., and K. Dementhon, 2006 Non-self recognition and programmed cell death in filamentous fungi. Curr. Opin. Microbiol. 9: 553–558.

Glass, N. L., and G. A. Kuldau, 1992 Mating type and vegetative incompatibility in filamentous ascomycetes. Annu. Rev. Phytopathol. 30: 201–224.

Glass, N. L., D. J. Jacobson, and P. K. T. Shiu, 2000 The genetics of hyphal fusion and vegetative incompatibility in filamentous ascomycete fungi. Annu. Rev. Genet. 34: 165–186.

Hall, C., J. Welch, D. J. Kowbel, and N. L. Glass, 2010 Evolution and diversity of a fungal self/nonself recognition locus. PLoS ONE 5: 14.

Hartl, D. L., E. R. Dempster, and S. W. Brown, 1975 Adaptive significance of vegetative incompatibility in *Neuorspora crassa*. Genetics 81: 553–569.

Heiniger, U., and D. Rigling, 1994 Biological control of chestnut blight in Europe. Annu. Rev. Phytopathol. 32: 581–599.

Hillman, B. I., R. Shapira, and D. L. Nuss, 1990 Hypovirulence-associated suppression of host functions in *Cryphonectria parasitica* can be partially relieved by high light intensity. Phytopathology 80: 950–956.

Hong, W., 2005 SNAREs and traffic. Biochim. Biophys. Acta 1744: 493–517.

Huber, D. H., 1996 Genetic analysis of vegetative incompatibility polymorphisms and horizontal transmission in the chestnut blight fungus *Cryphonectria parasitica*. Ph.D. Thesis, Michigan State University, East Lansing, MI.

Huber, D. H., and D. W. Fulbright, 1994 Preliminary investigations on the effect of individual genes upon the transmission of dsRNA in *Cryphonectria parasitica*, pp. 15–19 in *Proceedings of the International Chestnut Conference*, edited by M. L. Double and W. L. MacDonald. West Virginia University Press, Morgantown, WV.

Jacobson, D. J., K. Beurkens, and K. L. Klomparens, 1998 Micro scopic and ultrastructural examination of vegetative incompatibility in partial diploids heterozygous at *het* loci in *Neurospora crassa*. Fungal Genet. Biol. 23: 45–56.

Jahn, R., and R. H. Scheller, 2006 SNAREs—engines for membrane fusion. Nat. Rev. Mol. Biol. 7: 631–643.

Kaneko, I., K. Dementhon, Q. Xiang, and N. L. Glass, 2006 Nonalleic interactions between *het-c* and a polymorphic locus, *pin-c*, are essential for nonself recognition and programmed cell death in *Neurospora crassa*. Genetics 172: 1545–1555.

Kubisiak, T. L., and M. G. Milgroom, 2006 Markers linked to vegetative incompatibility (*vic*) genes and a region of high heterogeneity and reduced recombination near the mating type locus (*MAT*) in *Cryphonectria parasitica*. Fungal Genet. Biol. 43: 453–463.

Kubisiak, T. L., C. Dutech, and M. G. Milgroom, 2007 Fifty-three polymorphic microsatellite loci in the chestnut blight fungus, *Cryphonectria parasitica*. Mol. Ecol. Notes 7: 428–432.

Kuwayama, H., S. Obara, T. Morio, M. Katoh, H. Urushihara *et al.*, 2002 PCR-mediated generation of a gene disruption construct without the use of DNA ligase and plasmid vectors. Nucleic Acids Res. 15: E2.

Lan, X., Z. Yao, Y. Zhou, J. Shang, H. Lin *et al.*, 2008 Deletion of the *cpku80* gene in the chestnut blight fungus, *Cryphonectria parasitica*, enhances gene disruption efficiency. Curr. Genet. 53: 59–66.

Leslie, J. F., 1993 Fungal vegetative compatibility. Annu. Rev. Phytopathol. 31: 127–150.

Leslie, J. F., and K. A. Zeller, 1996 Heterokaryon incompatibility in fungi: more than just another way to die. J. Genet. 75: 415–424.

MacDonald, W. L., and D. W. Fulbright, 1991 Biological control of chestnut blight: use and limitations of transmissible hypovirulence. Plant Dis. 75: 656–661.

Margulies, M., M. Egholm, W. E. Altman, S. Attiya, J. S. Bader *et al.*, 2005 Genome sequencing in microfabricated high-density picolitre reactors. Nature 437: 376–380.

Micali, C. O., and M. L. Smith, 2006 A nonself recognition gene complex in *Neurospora crassa*. Genetics 173: 1991–2004.

Milgroom, M. G., and P. Cortesi, 1999 Analysis of population structure of the chestnut blight fungus based on vegetative incompatibility genotypes. Proc. Natl. Acad. Sci. USA 96: 10518–10523.

Milgroom, M. G., and P. Cortesi, 2004 Biological control of chestnut blight with hypovirulence: a critical analysis. Annu. Rev. Phytopathol. 42: 311–338.

Nuss, D. L., 1992 Biological control of chestnut blight: an example of virus-mediated attenuation of fungal pathogenesis. Microbiol. Rev. 56: 561–576.

Nuss, D. L., 2005 Hypovirulence: mycoviruses at the fungal-plant interface. Nat. Rev. Microbiol. 3: 632–642.

Nuss, D. L., 2010 Mycoviruses, pp. 145–152 in *Cellular and Molecular Biology of Filamentous Fungi*, edited by K. A. Borkovich, and D. J. Ebbole. ASM Press, Washington, DC.

Paoletti, M., and C. Clave, 2007 The fungus-specific HET domain mediates programmed cell death in *Podospora anserina*. Eukaryot. Cell 6: 2001–2008.

Paoletti, M., and S. J. Saupe, 2009 Fungal incompatibility: evolutionary origin and pathogen defense? BioEssays 31: 1201–1210.

Paoletti, M., S. J. Saupe, and C. Clave, 2007 Genesis of a fungal non-self recognition repertoire. PLoS ONE 2: e283.

Pearson, M. N., R. E. Beever, B. Boine, and K. Arthur, 2009 Mycoviruses of filamentous fungi and their relevance to plant pathology. Mol. Plant Pathol. 10: 115–128.

Pinan-Lucarre, B., M. Paoletti, and C. Clave, 2007 Cell death by incompatibility in the fungus *Podospora*. Semin. Cancer Biol. 17: 101–111.

Powell, W. A., 1995 Vegetative incompatibility and mycelial death of *Cryphonectria parasitica* detected with a pH indicator. Mycologia 87: 738–741.

Richman, A., 2000 Evolution of balanced genetic polymorphism. Mol. Ecol. 9: 1953–1963.

Robin, C., C. Anziani, and P. Cortesi, 2000 Relationship between biological control, incidence of hypovirulence, and diversity of vegetative incompatibility types of *Cryphonectria parasitica* in France. Phytopathology 90: 730–737.

Robin, C., X. Capdeville, M. Martin, C. Traver, and C. Colinas, 2009 *Cryphonectria parasitica* vegetative compatibility type analysis of populations in south-western France and northern Spain. Plant Pathol. 58: 527–535.

Root, C., C. Balbalian, R. Bierman, L. M. Geletka, S. Anagnostakis *et al.*, 2005 Multi-seasonal field release and spermatization trials of transgenic hypovirulent strains of *Cryphonectria parasitica* containing cDNA copies of hypovirulent CHV1–EP713. For. Pathol. 35: 277–297.

Saupe, S. J., 2000 Molecular genetics of heterokaryon incompatibility in filamentous ascomycetes. Microbiol. Mol. Biol. Rev. 64: 489–502.

Saupe, S. J., B. Turcq, and J. Bégueret, 1995 Sequence diversity and unusual variability at the *het-c* locus involved in vegetative

incompatibility in the fungus *Podospora anserina*. Curr. Genet. 27: 466–471.
Saupe, S. J., C. Clavé, and J. Bégueret, 2000 Vegetative incompatibility in filamentous fungi: *Podospora* and *Neurospora* provide some clues. Curr. Opin. Microbiol. 3: 608–612.
Segers, G. C., X. Zhang, F. Deng, Q. Sun, and D. L. Nuss, 2007 Evidence that RNA silencing functions as an antiviral defense mechanism in fungi. Proc. Natl. Acad. Sci. USA 104: 12902–12906.
Smith, M. L., C. C. Gibbs, and M. G. Milgroom, 2006 Heterokaryon incompatibility function of barrage-associated vegetative incompatibility genes (*vic*) in *Cryphonectria parasitica*. Mycologia 98: 43–50.
Sun, Q., G. H. Choi, and D. L. Nuss, 2009a Hypovirus-responsive transcription factor gene *pro1* of the chestnut blight fungus *Cryphonectria parasitica* is required for female fertility, asexual spore development, and stable maintenance of hypovirus infection. Eukaryot. Cell 8: 262–270.
Sun, Q., G. H. Choi, and D. L. Nuss, 2009b A single Argonaute gene is required for induction of RNA silencing antiviral defense and promotes viral RNA recombination. Proc. Natl. Acad. Sci. USA 106: 17927–17932.
Suzuki, N., K. Maruyama, M. Moriyama, and D. L. Nuss, 2003 Hypovirus papain-like protease p29 functions *in trans* to enhance viral double-stranded RNA accumulation and vertical transmission. J. Virol. 77: 11697–11707.
Van Alfen, N. K., R. A. Jaynes, S. L. Anagnostakis, and P. R. Day, 1975 Chestnut blight: biological control by transmissible hypovirulence in *Endothia parasitica*. Science 189: 890–891.
Wickner, R. B., 2001 Viruses of yeasts, fungi and parasitic microorganisms, pp. 629–658 in *Fields Virology*, 4th Ed., edited by D. M. Knipe, and P. M. Howley. Lippincott Williams & Wilkins, Philadelphia.
Wu, J., S. J. Saupe, and N. L. Glass, 1998 Evidence for balancing selection operating at the het-c heterokaryon incompatibility locus in a group of filamentous fungi. Proc. Natl. Acad. Sci. USA 95: 12398–12403.
Zhang, X., G. C. Segers, Q. Sun, F. Deng, and D. L. Nuss, 2008 Characterization of hypovirus derived small RNAs generated in the chestnut blight fungus by an inducible DCL-2 dependent pathway. J. Virol. 82: 2613–2619.

Communicating editor: E. U. Selker

GENETICS

Supporting Information
http://www.genetics.org/content/suppl/2011/10/20/genetics.111.133983.DC1

Molecular Characterization of Vegetative Incompatibility Genes That Restrict Hypovirus Transmission in the Chestnut Blight Fungus *Cryphonectria parasitica*

Gil H. Choi, Angus L. Dawe, Alexander Churbanov, Myron L. Smith, Michael G. Milgroom, and Donald L. Nuss

DOI: 10.1534/genetics.111.133983

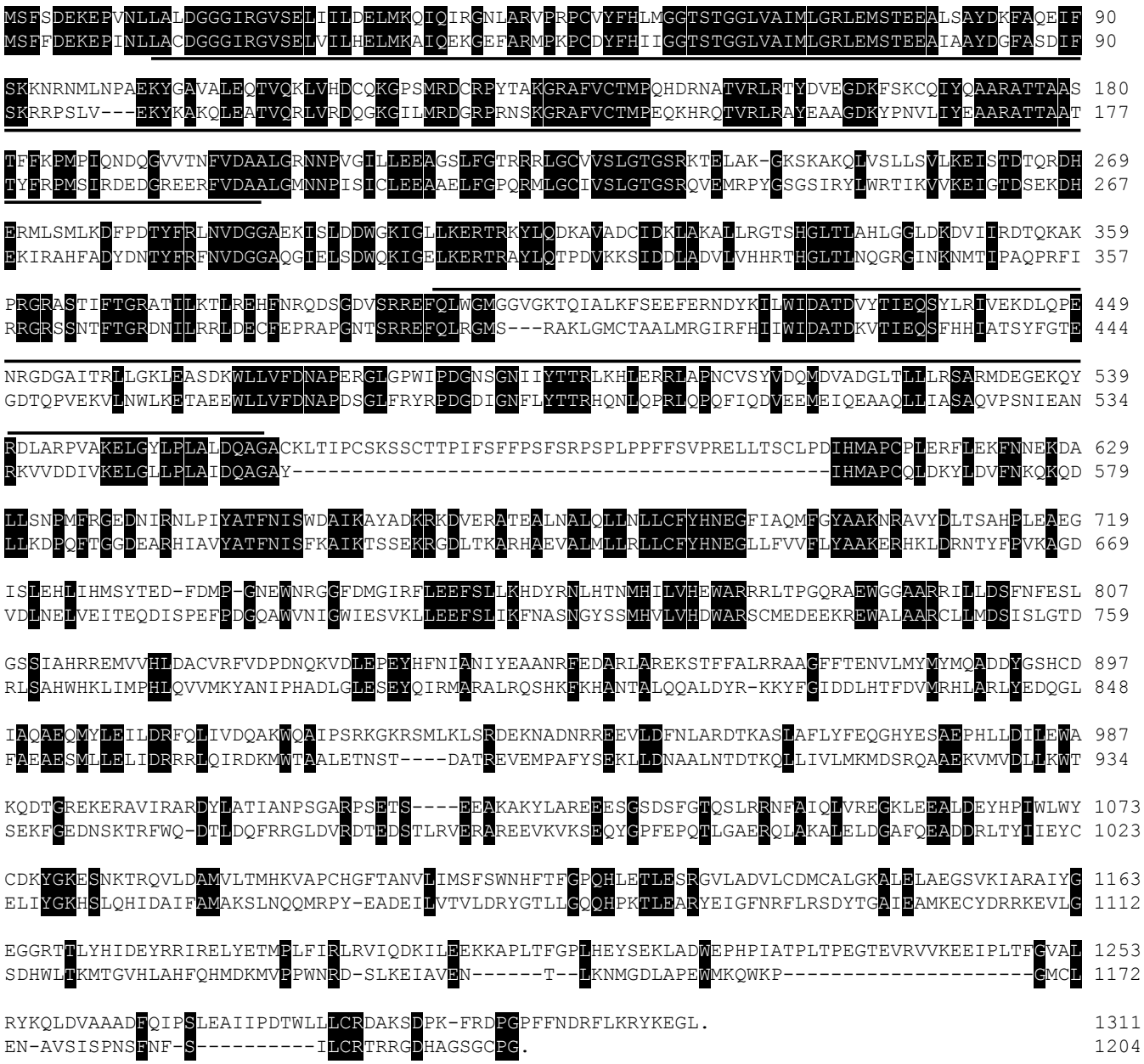

Figure S1 Amino acid alignment of candidate *vic2* alleles in strain EP155 (*vic2-2*) and in strain EP146 (*vic2-1*) performed using MegAlign in Lasergene (DNASTAR Inc. Madison WI). Note the high level of polymorphism that spans nearly all of the patatin-like protein (39% identity). A region in the N-terminal portion of the ORF (aa 13-212 in the EP155 sequence) containing a patatin-like phospholipase domain (PLA2; EC3.1.1.4) consisting of the esterase box GTSTG and anion binding element DGGGXRG (Scherer et al., 2010 Patatin-related phopholipase A: nomenclature, subfamilies and functions in plants. *Trends in Plant Science* **15**:693-700), and conserved in both the *vic2-1* and *vic2-2* alleles, is underlined. An NB-ARC, or P-loop NTPase domain, detected in the EP155 genome sequence but not in the EP146 sequence, is indicated by an overline extending from aa 396-561. Amino acid identity is indicated by the solid background, while dashes indicate deletion events.

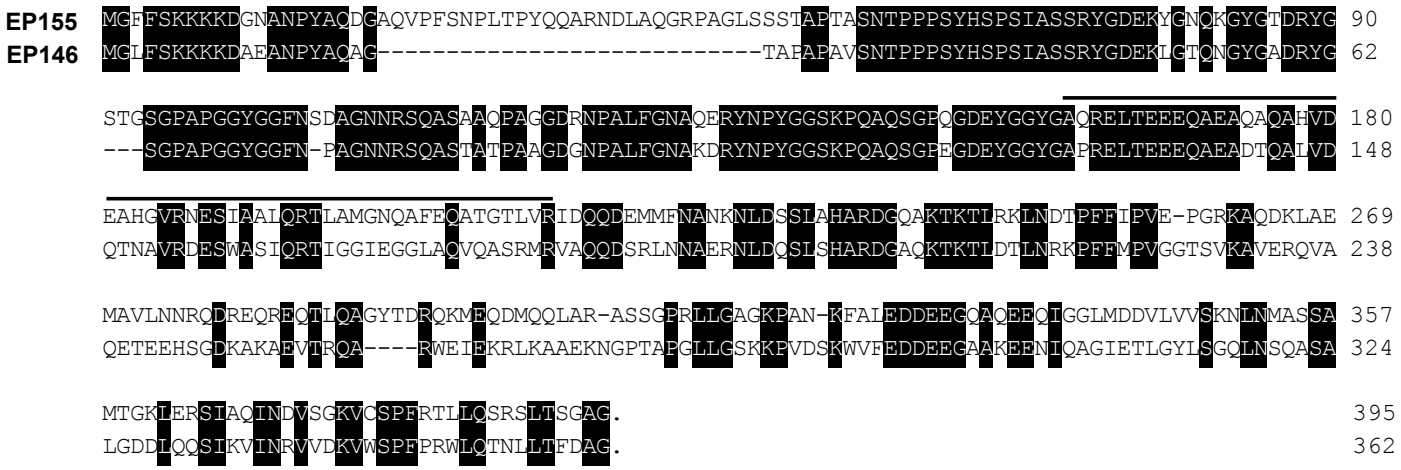

Figure S2 Amino acid alignment of the Sec9-like protein candidate *vic2a* alleles in strain EP155 (*vic2a-2*) and EP146 (*vic2a-1*). Note the large indel near the N-terminus and the high level of polymorphism in the C-terminal half of the coding region. A Pfam DUF3359 domain, found only in the EP155 allele, is indicated by a line above the EP155 sequence. Amino acid identity is indicated by the solid background, while dashes indicate indels.

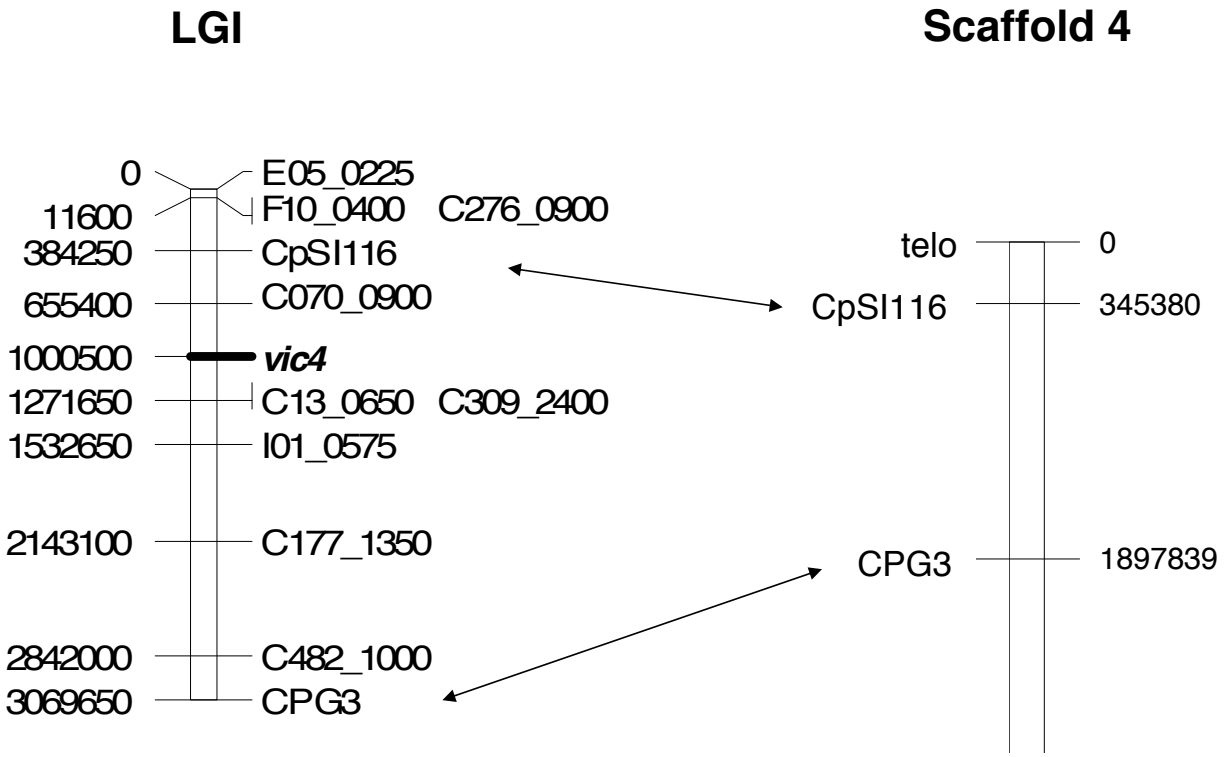

Figure S3 Alignment of linkage group LGI of the *C. parasitica* genetic linkage map generated by Kubisiak TL, Milgroom MG (2006 *Fungal Genetics and Biology* **43**: 453-463) that contains the position of the *vic4* genetic locus with Scaffold 4 of version 2 of the *C. parasitica* genome sequence. The estimated physical distance (bp) of each marker from the end of the linkage group (shown on the left side of the linkage map) was calculated using the estimate of 1cM = 14.5 kbp (Kubisiak and Milgroom, 2006 *Fungal Genetics and Biology* **43**: 453-463). Markers linking the physical and genetic maps are connected by double arrows.

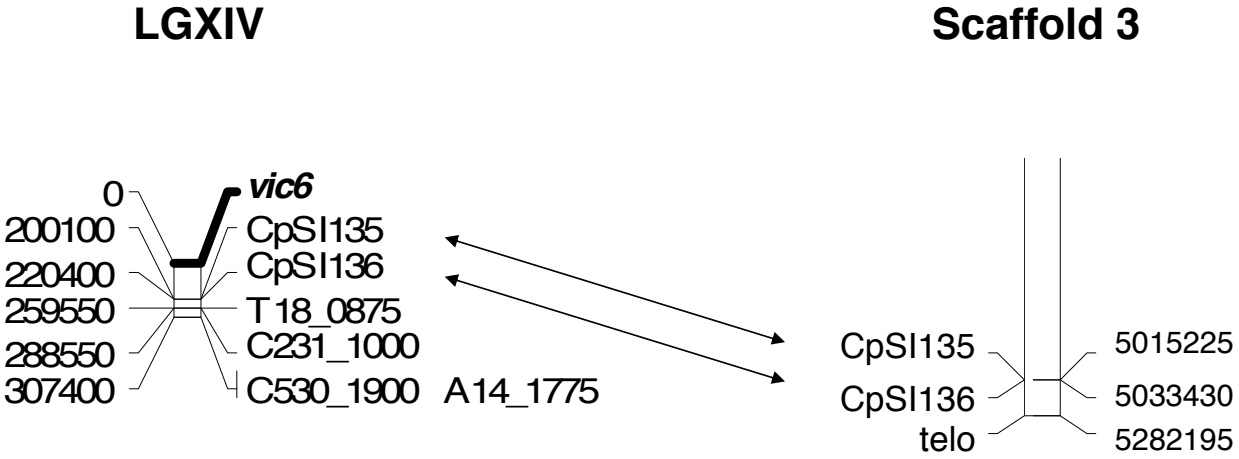

Figure S4 Alignment of linkage group LGXIV of the *C. parasitica* genetic linkage map generated by Kubisiak and Milgroom (2006 *Fungal Genetics and Biology* **43**: 453-463) that contains the position of the *vic6* genetic locus with Scaffold 3 of version 2 of the *C. parasitica* genome sequence. The estimated physical distance (bp) of each marker from the end of the linkage group (shown on the left side of the linkage map) was calculated using the estimate of 1cM = 14.5 kbp (Kubisiak and Milgroom, 2006 *Fungal Genetics and Biology* **43**: 453-463). Markers linking the physical and genetic maps are connected by double arrows.

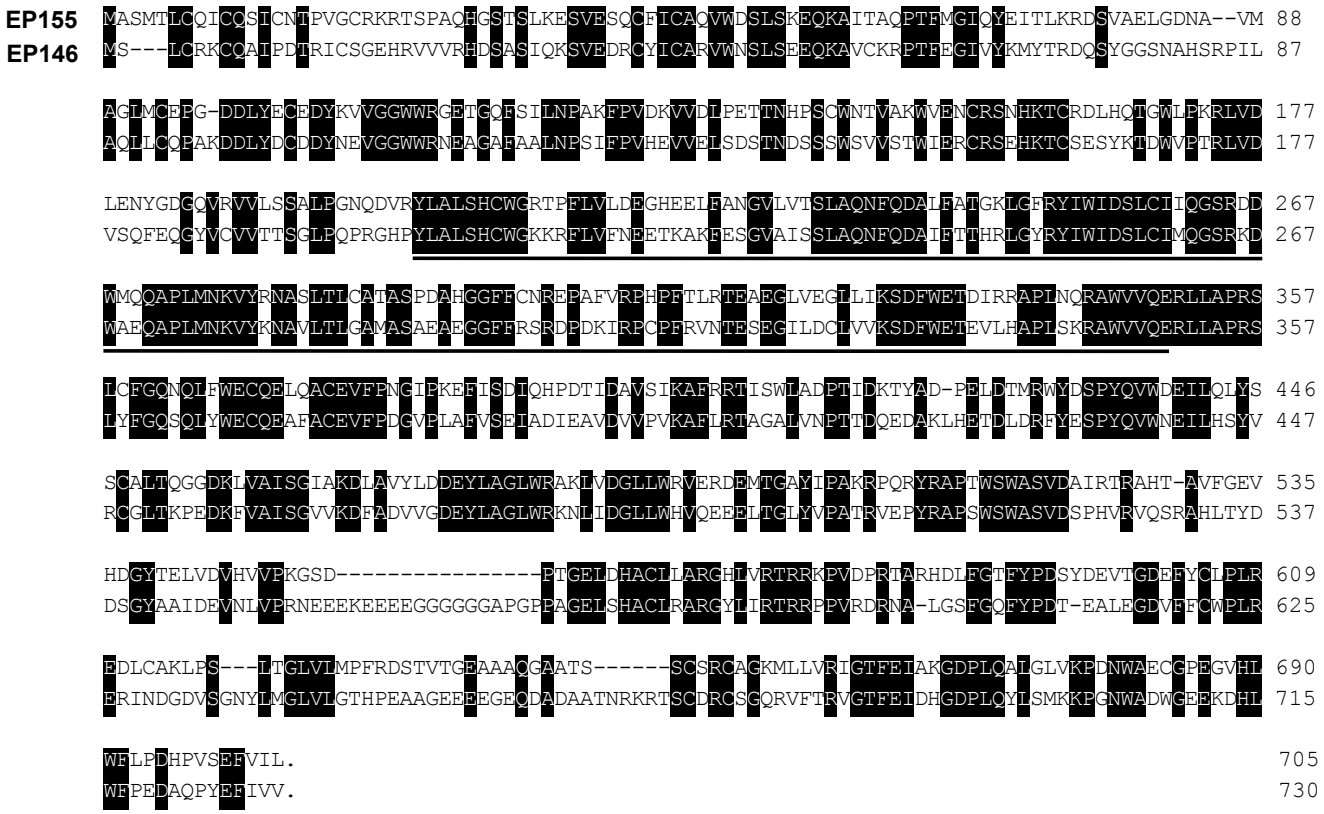

Figure S5 Amino acid alignment of *vic6* alleles in strain EP155 (*vic6-2*) and in strain EP146 (*vic6-1*). Note the high level of polymorphism that spans nearly all of the predicted protein (53% identity). The conserved HET domain found in this candidate *vic* gene is underlined. Amino acid identity is indicated by the solid background, while dashes indicate indels.

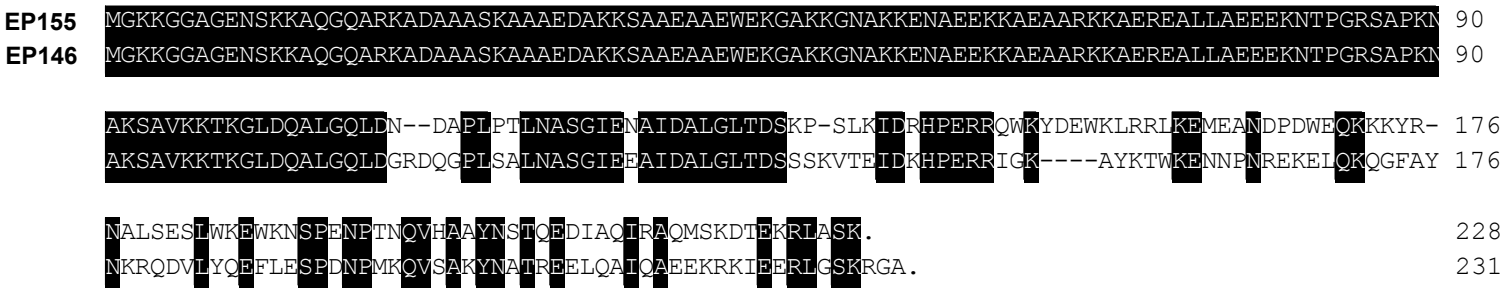

Figure S6 Amino acid alignment of alleles *pix6-1* and *pix6-2* in strains EP146 and EP155, respectively. Note the highly conserved N-terminal region and highly polymorphic C-terminal region. Amino acid identity is indicated by the solid background, while dashes indicate indels.

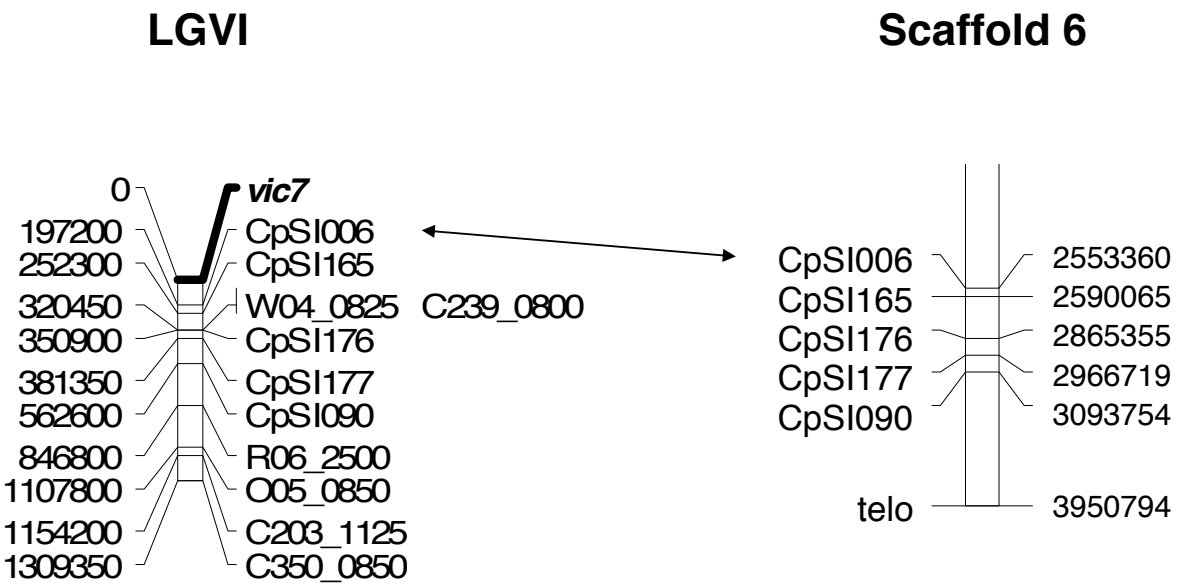

Figure S7 Alignment of linkage group LGVI of the *C. parasitica* genetic linkage map generated by Kubisiak and Milgroom (2006 *Fungal Genetics and Biology* **43**: 453-463) that contains the position of the *vic7* genetic locus with Scaffold 6 of version 2 of the *C. parasitica* genome sequence. The estimated physical distance (bp) of each marker from the end of the linkage group (shown on the left side of the linkage map) was calculated using the estimate of 1cM = 14.5 kbp (Kubisiak and Milgroom, 2006 *Fungal Genetics and Biology* **43**: 453-463)). Markers linking the physical and genetic maps are connected by double arrows.

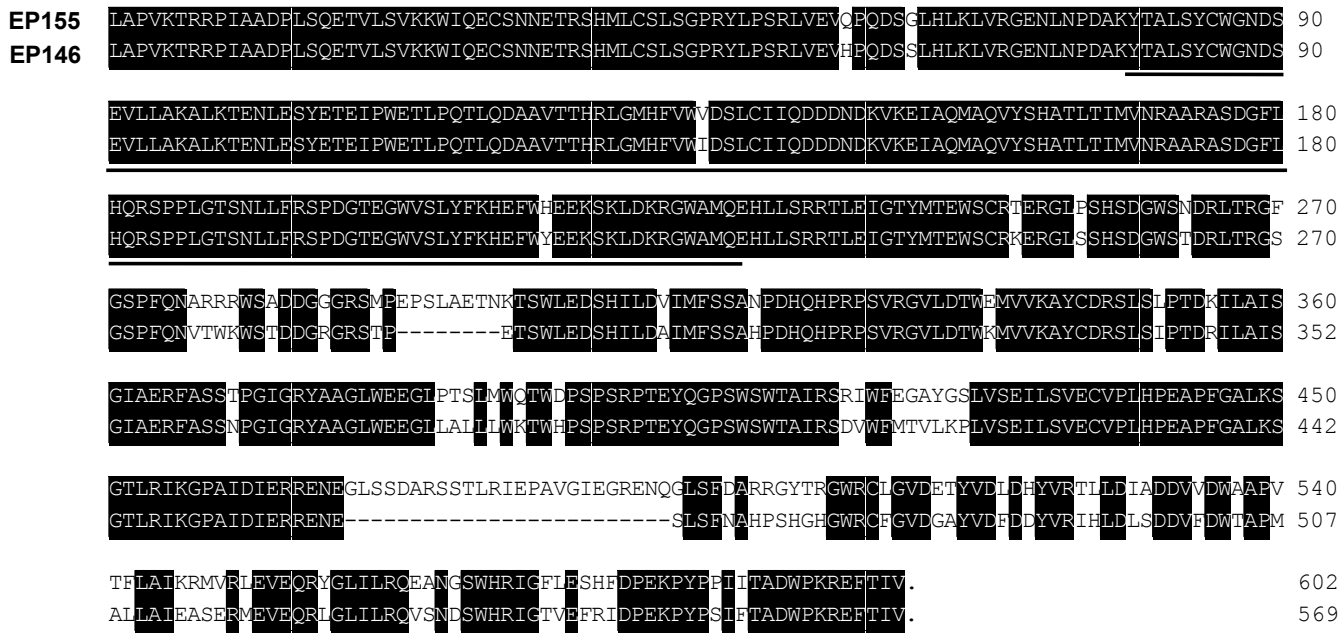

Figure S8 Amino acid alignment of candidate *vic7* alleles in strain EP155 (*vic7-2*) and in strain EP146 (*vic7-1*). The alignment was performed using MegAlign in Lasergene (DNASTAR Inc., Madison WI) with manually annotated amino acid sequences. Note that, in contrast to *vic2, vic4,* and *vic6*, the *vic7* alleles are quite similar to each other, except in the C-terminal region. The conserved HET domain found in this candidate *vic* gene is underlined.

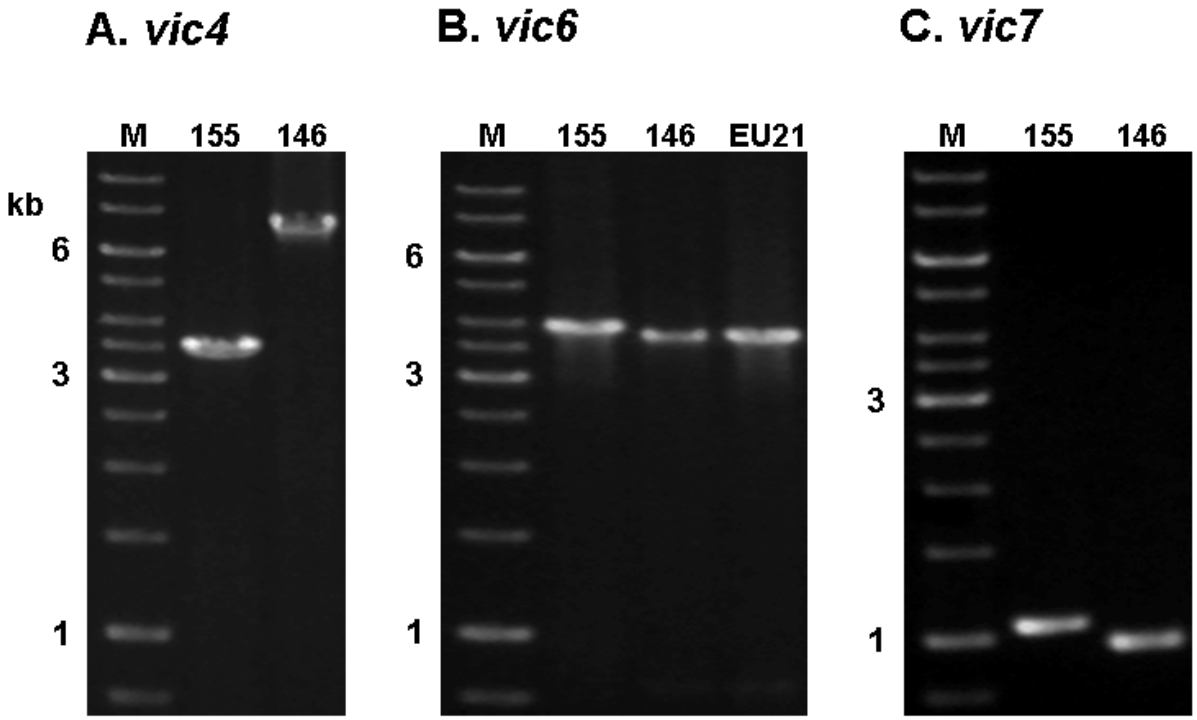

Figure S9 Agarose gel migration of candidate *vic* allele-specific PCR fragments. The relative migration positions of PCR products for *vic4-2* (3,456 bp from strain EP155 DNA) and *vic4-1* (6,884 bp strain EP146 DNA) are shown in Panel A. The candidate *vic6* allele-specific PCR product *vic6-1* (3,780 from strain EP146 and *vic* tester strain EU-21 DNAs) migrates slightly faster than the *vic6-2* PCR product (3,948 bp from EP155 DNA) as indicated in Panel B. Confirmatory nucleotide sequence analysis of PCR fragments was performed when differentiation based on relative migration was in doubt. The migration positions for candidate *vic7* allele-specific PCR products for *vic7-2* (1,053 bp from EP155 DNA) and *vic7-1* (954 bp from EP146 DNA) are shown in Panel C. Nucleotide sequence differences were also used to distinguish the candidate *vic2-1* and *vic2-2* alleles and the adjacent sec9-like gene alleles *vic2-1a* and *vic2-2a*. The lanes marked M contained the 1 Kbp DNA ladder size markers (Fermentas, Glen Burnie, MD).

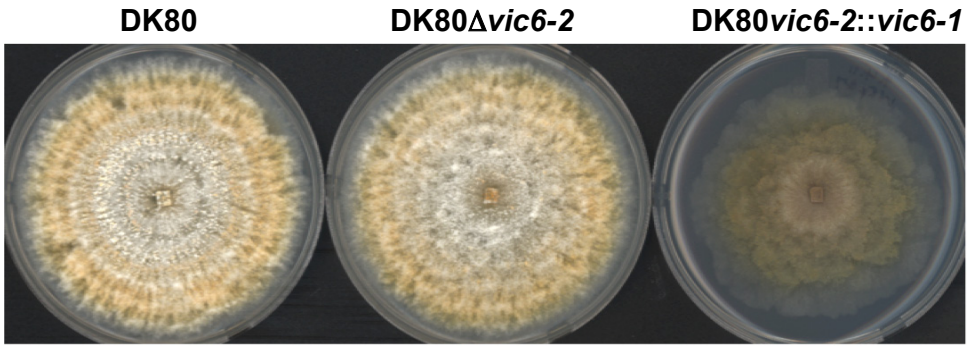

Figure S10 Colony morphology for disruption strain DK80 *Δvic6-2* (middle panel) and replacement strain DK80 *vic6-2*::*vic6-1* (right panel) in which the disrupted *vic6-2* allele was replaced with an intact *vic6-1* gene. The *vic6-1* replacement strain DK80 *vic6-2*::*vic6-1* exhibited abnormal colony morphology, irregular margins, reduced aerial hyphae, reduced biomass production and reduced conidiation. All candidate *vic* gene disruption mutants examined in this study showed normal colony morphology.

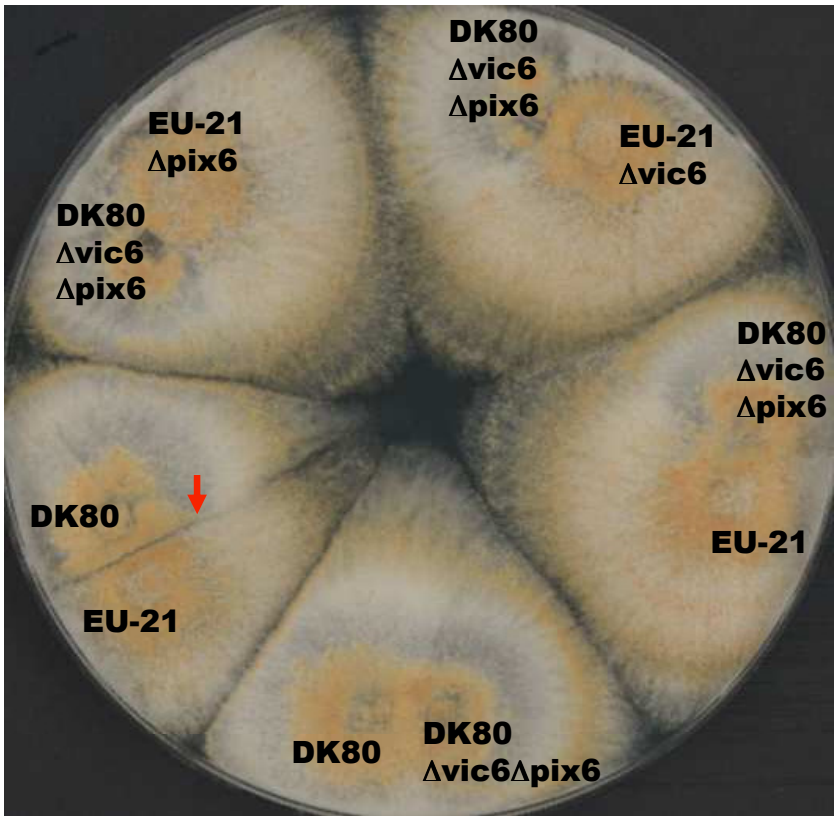

Figure S11 Mycelial incompatibility assay for strain DK80 disrupted in *pix6-2* and *vic6-2*. Barrage formation (arrow) resulting from an incompatible reaction between strains DK80 and EU-21 that differ only at the *vic6* locus is shown in at the lower left. While barrage formation is retained when only *vic6* or *pix6* alleles are independently disrupted (Table 5), the double disruption mutant DK80 *Δpix6-2 Δvic6-2* is compatible with strain EU-21 with no evidence of barrage formation (middle right) and no restriction to virus transmission in either directions (Table 5).

Table S1 Single Sequence Repeat (SSR) linkage markers used in this study

Linkage Marker	*vic*	Forward primer	Reverse primer	Scaffold map positions*
CpSI002	*vic2*	TTGGATAGACCCAGGTGTCC	GAGGTCTTCGAGGGCGTAG	7:1522713-1523193
Co16_1800	*vic2*	TGGCGGGATATGAAATAT	TGTTGGAGCGCCTTGCGGA	7:1762655-1763779
CpSI116	*vic4*	TGTCAAAGTTGACCACCACC	ATCAGCGTGTCCATACCACA	4:345343-345591
CPG3	*vic4*	CGTAAGGCAGAGGCAGAGAC	TCCCTATGCCCAAGACACTC	4:1897980-1898174
CpSI135	*vic6*	TACTCTTCGTGTCCCTTCGG	GGCAGAACAGTGACCGAAAT	3:5015099-5015384
CpSI136	*vic6*	AAGCTGTACAGTCAACGCGA	ACCTGGAATGGAGACACAGG	3:5033364-5033641
CpSI006	*vic7*	ATGTCGAGTTTACCCGATGG	GAGATGTGTGGAATGCAACG	6:2553319-2553459

* The map positions define the fragment containing the SSR region that would be amplified from *C. parasitica* genomic DNA. (KUBISIAK T. L., C. DUTECH and M. G. MILGROOM, 2007 Fifty-three polymorphic microsatellite loci in the chestnut blight fungus, *Cryphonectria parasitica*. Mol. Ecol. Notes **7**: 428-432)

Table S2 Oligonucleotide primers used in PCR reactions*

Gene	Primer	Nucleotide sequence
vic2	ptnF1	5′-TGCGGCACCTGCATGTACATA
	ptnR1	5′-CGTCATACAGGCGAACTGGAT
vic2a	sec9F1	5′-TACTCCTTCCCAAGCTCCCG
	sec9R1	5′-GCTCAACGTATGTGGTTCAGCAT
vic4	vic4F1	5′-CCATGCATGTGAGGCTTCTCA
	vic4R1	5′-CTTGATCGTGGAGTTCAGTCG
vic6	vic6F1	5′-GACCAGGCTCTTGGGCAGCT
	vic6R1	5′-CGAGACCCTTTGTTTCTAAGGTCT
pix6	vic6upF1	5′-GTGCAGGTCCAGCTGACTTG
	vic6up155R1	5′-TGTACAGCGTGGCCACTGAC
	vic5up146R1	5′-AGGCCTTTGAGGATGGGGTT
vic7	vic7F1	5′-CGTACACTTGAGATTGGGACTTA
	vic7R1	5′-ATAGGGCTTCTCGGGATCGA

*A Phire Plant Direct PCR kit (F-130) (New England BioLabs, Ipswich, MA) was employed in a 50 μl reaction volume with following parameters: denaturation at 98^0 C for 2 min followed by 30 cycles consisting of denaturation at 98^0 C for 5 sec, annealing at 64^0 C for 5 sec, extension at 72^0 C for 2.5 min, and then final extension at 72^0 C for additional one minute. The resulting PCR products were sequenced after purification with a QIAquick PCR purification kit (Qiagen, Valencia, CA).